Palacký University
Olomouc

Self-organized biopolymer layers and coatings with mineral fillers for special applications

MSc. Yousef Murtaja

Summary of Ph.D. Dissertation in Nanomaterials Chemistry

Supervisor: Prof. Ing. Lubomír Lapčík, Ph.D.

Department of Physical Chemistry, UPOL

Olomouc 2023

Faculty
of Science

Palacký University
Olomouc

Contents

The dissertation was prepared as part of the doctoral studies in Nanomaterials Chemistry at the Department of Physical Chemistry, Faculty of Science, Palacký University in Olomouc.

Ph.D. student: MSc. Yousef Murtaja

Department of Physical Chemistry, UPOL

Supervisor: Prof. Ing. Lubomír Lapčík, Ph.D.

Department of Physical Chemistry, UPOL

Opponents:

Place and date of defense:

Please note: Opponents and a place where it will be possible to get acquainted with the dissertation and the assessments at least 14 days before the defense.

Abstract

This dissertation emphasizes the application of mineral fillers in natural biopolymer layers for specific purposes, polymer composites, and nanofillers and their properties. The thesis is presented as a collection of scientific research in the form of thematically arranged published papers, supported by an annotated theoretical framework. Alternatives to artificial coatings are available in natural biopolymers with added mineral fillers, which are environmentally friendly and sustainable in the long term. Integrating mineral fillers into these coatings can improve their properties to meet specific application requirements. Nanofillers added to polymer composites can improve mechanical strength and resistance to high temperatures without any degradation effect.

The first research paper confirms that perlite plays a key role in the thermal and mechanical properties of HDPE-based nanocomposite materials. Young's tensile modulus increases with increasing filler material concentration, leading to an increase in stiffness. The degree of fracture toughness decreases with increasing concentration of perlite at brittle fracture. However, higher concentrations of filler material are also associated with the measured ductile fracture behavior. SEM analysis confirms the strong bonding between the polymer matrix chains and the filler particle.

Further research revealed the effect of two different types of inorganic mineral fillers, calcium carbonate nanoparticles, and mineral nano silicates (nano clay), on the mechanical behavior of HDPE nanocomposite polymers in a semi-operational test. The study focuses on the characterization of fillers uniformly dispersed in the samples using SEM imaging techniques, X-ray analysis of dispersion spectra, and the TEM method. However, the addition of these fillers improves the technical properties of the polymer composites as shown by the combination of the elastic modulus and the microhardness observed. The amount and extent of fillers in the composites determine their elastic mechanical behavior and plasticity.

The technical properties of epoxy/HNTs & GnPs composites are the focus of the third research study. These shows that planar particles exhibit mutual sliding during mechanical testing, thereby reducing the overall stiffness of GnPs nanocomposites and increasing their ductility and plasticity. The stiffness of epoxy/HNT composites decreases with the addition of nanofiller, as indicated by the observed lower Young's modulus in tension. The study reveals the different mechanical responses of the tested materials due to the ductile and brittle fracture processes occurring.

In addition, the resistance of polyurethane foams to thermal degradation, including thermal stress-induced changes in their mechanical properties, is studied using selected physicochemical methods. The effect of increased relative humidity on degradation, leading to a decrease in stiffness and permanent deformation, was also found. In addition, the dynamic-mechanical properties of the studied composite materials were investigated by measuring the vibration damping excited by a single degree of freedom oscillatory system (SDOF). In this way, the changes in elasticity caused by different conditioning of the studied samples, which led to progressive degradation and loss of thermal stability, were monitored.

In summary, this dissertation provides valuable insights into the latest research trends and developments in natural biopolymer films with mineral fillers, their properties, and potential applications. The results of the studies in this dissertation provide important data for the design of sustainable and environmentally friendly materials for specific needs and offer possible directions for scientific developments in the field of polymer composites and nanofillers.

Abstrakt

Disertační práce klade důraz na aplikaci minerálních plniv do přírodních biopolymerních vrstev pro specifické účely, dále na polymerní kompozity a nanoplniva a také na jejich vlastnosti. Práce je prezentována jako souhrn vědeckého výzkumu formou tematicky uspořádaných publikovaných odborných článků, podpořených komentovaným teoretickým rámcem. Alternativy k umělým nátěrům jsou dostupné v přírodních biopolymerech s přísadami minerálních plniv, které jsou šetrné k životnímu prostředí a dlouhodobě udržitelné. Integrace minerálních plniv do těchto nátěrů může zlepšit jejich vlastnosti, aby vyhovovaly specifickým aplikačním požadavkům. Nanoplniva přidaná do polymerního kompozitu mohou zlepšit mechanickou pevnost a odolnost vůči vysokým teplotám bez jakéhokoli degradačního účinku.

První výzkumný článek potvrzuje, že perlit hraje klíčovou roli v tepelných a mechanických vlastnostech nanokompozitních materiálů na bázi HDPE. Youngův modul pružnosti v tahu se zvyšuje s rostoucí koncentrací výplňového materiálu, což vede ke zvýšení tuhosti. Stupeň lomové houževnatosti klesá s rostoucí koncentrací perlitu při křehkém lomu. Nicméně vyšší koncentrace plniva jsou také spojeny s naměřeným průběhem tvárného lomu. Analýza SEM potvrzuje silnou vazbu mezi řetězci polymerní matrice a částicí plniva.

Další výzkum odhalil vliv dvou různých typů anorganických minerálních plniv, nanočástic uhličitanu vápenatého a minerálních nanosilikátů na mechanické chování nanokompozitních polymerů HDPE v poloprovozním testu. Studie se zaměřuje na charakterizaci plniv rovnoměrně rozptýlených ve vzorcích pomocí zobrazovacích technik SEM, RTG analýzou disperzních spekter a metodou TEM. Přidání těchto plniv však zlepšuje technické vlastnosti polymerních kompozitů, jak ukazuje kombinace modulu pružnosti a zjištěné mikrotvrdosti. Množství a rozsah plniv v kompozitech určují jejich elastické mechanické chování a plasticitu.

Technické vlastnosti epoxidových/HNTs & GnPs kompozitů jsou středem zájmu třetí výzkumné studie. Tato ukazuje, že planární částice vykazují vzájemné klouzání v průběhu mechanického testování a tím snižují celkovou tuhost GnPs nanokompozitů a zvyšují jejich tažnost a plasticitu. Tuhost epoxidových/HNT kompozitů klesá přídavkem nanoplniva, což naznačuje zjištěný nižší Youngův modul pružnosti v tahu. Studie odhaluje různé mechanické odezvy zkoušených materiálů v důsledku vznikajících tvárných i křehkých lomových dějů.

Dále je pomocí vybraných fyzikálně-chemických metod studována odolnost polyuretanových pěn vůči tepelné degradaci včetně změn jejich mechanických vlastností indukovaných tepelným namáháním. Byl zjištěn také vliv zvýšené relativní vlhkosti na degradaci, vedoucí ke snížení tuhosti a permanentní deformace. Dále byly proměřeny dynamicko-mechanické vlastnosti studovaných kompozitních materiálů metodou měření útlumu vibrací vybuzených oscilačním systémem o jednom stupni volnosti (SDOF). Tímto způsobem byly sledovány změny elasticity způsobené různým kondicionováním studovaných vzorků, které vedly k postupné degradaci a ztrátě tepelné stability.

V souhrnu, tato disertační práce poskytuje cenné poznatky o nejnovějších výzkumných trendech a vývoji v oblasti přírodních biopolymerních vrstev s minerálními plnivy, jejich vlastnostech a potenciálních aplikacích. Výsledky studií této disertační práce poskytují důležitá data pro tvorbu udržitelných a ekologicky šetrných materiálů pro specifické potřeby a nabízí možné směry vědeckého vývoje v oblasti polymerních kompozitů a nanoplniv.

1. Introduction

All-natural biopolymers are now a promising solution for satisfying the increasing need for polymeric materials and also addressing environmental issues. Natural biopolymers are employed in daily life and many industries including engineering and medicine, defense, and cars, allowing them to cross-link and produce lasting and revolutionary components. With decreased economic variability, light polymer composites can tackle power use and high price concerns in industries heavily reliant on heavy building materials. Furthermore, substantial research is performed to enhance the qualities of biopolymers to minimize waste as well as carbon emissions in materials-based industries. Biopolymers derived from natural sources possess specific qualities because they can naturally appear inside living organisms, call for no extra treatment just before use, happen in different physical forms solid, solution, semi-solid, and are capable to make thin layers on solid surfaces. These characteristics render them appropriate for utilization in the region of printing arts, the packaging market, the textile market, and other industries. (1-3). Natural, renewable, and plentiful, cellulose is a complex polymer with linear glucose-built alongside with polysaccharides. It also offers nourishment to numerous organisms such as Algae, bacteria, and plant cells. (Figure 1.a) During the 1920s, carboxymethyl cellulose (CMC) (Figure 1.b) acquired considerable manufacturing significance. Its discovery exposed its enormous potential in different industries like food industries, textiles, paper, and drug sectors largely because of its economical manufacturing process and high effectiveness. Nitrocellulose (NC) is a rich natural cellulose derivative employed in printing inks, coatings, filter media, and biochemistry (5-7). Oxycellulose (OC) is a chemically risk-free organic polymer that breaks down easily and is compatible biologically (8,9). It finds application in surgical operations (10). The chemical substance hydroxyethyl cellulose (HEC) (another derivative of cellulose) is a well-known component of pharmaceuticals, skin care products as well as food businesses (Figure 1.c). It isn't toxic, non-ionic, and hydrophilic (11,12).

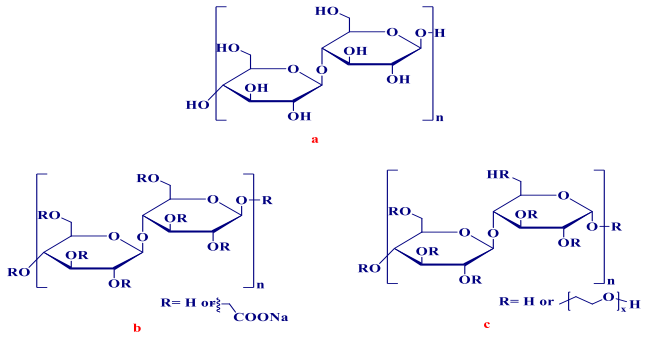

Figure 1. *(a) The structural formula of cellulose (b) The material configuration of carboxymethyl cellulose together with sodium salt (c) The composition structural of hydroxyethyl cellulose.*

HEC coatings possess the superior capability to form a film, and their ability to break down naturally and harmonize with biological systems makes them suitable for various biomedical uses. (13) Therefore, thoroughly examining diffusion and diffusion aspects of swelling and dissolution in the bio-polymers mentioned above, specifically CMC and also HEC, can contribute to advancing the growth of contemporary industries that heavily rely on these bio-polymers. Poly(ethylene) is a popular semicrystalline polymer that is extensively utilized because of its affordable price and distinctive physiochemical characteristics. The HDPE

nanocomposites demonstrate significant strength in their overall mechanical properties. The difference in elasticity modulus between the filler nanoparticles and polymer matrix results in a much better likelihood of cavity formation (14-18). The usage of inorganic mineral nano-fillers is growing in popularity as a means to enhance the performance of polymers like HDPE, particularly in terms of their ability to withstand wear and tear (19,20). The inclusion of these additives can alter the physiochemical behaviors of polymers, impacting their ability to wear durability wear and rupture, their surface strength, and their resilience and ductility (20). The addition of tiny particles to thermoplastic polymers resulted in enhancements in characteristics such as air permeability, elasticity, mechanical strength, rigidity and stiffness (21-24). Mineral fillers like perlite have been found to enhance the thermal stability and sound absorption aspects of polyesters (25-28). It is essential to comprehend how the performance of composites in consumer products and industries is affected by the polymer matrix and filler particles (28,29). The semi-crystalline polymers contain interconnected spherulites that make up the crystalline portion (30). Current studies suggest that the properties of thermoplastic polymer materials, including their mechanical characteristics and the mechanism they melt and crystallize, are greatly affected by the type, shape, and size of mineral fillers (31). According to reference (32), the overall effectiveness of mineral fillers in composite applications is impacted by factors such as the size, shape, and dispersion of the filler particles. To ensure a high level of consistency in producing biopolymer composites, it might be essential to perform mechanical evaluations on the materials obtained from commercially available fillers. The incorporation of nanofillers like GnPs and HNPs, along with an appropriate polymer matrix, can greatly enhance the durability (toughness) of the substances (33,34). Polymer composites such as polyester, polyurethane, and epoxy were recognized for their extraordinary mechanical strength and ability to absorb moisture, as well as their minimal shrinkage and reduced emission of toxic substances during the treating process (35-37). Although the tribological characteristics of epoxy resin are restricted, its influence on mechanical durability has made it a favored option in industrial settings. In biopolymers with differing properties, HNTs and GnPs function as highly effective nanofillers. GnPs possess excellent thermal stability, conductivity, fracture toughness, as well as enhance lubrication. On the other hand, HNTs exhibit a greater dispersion ratio and have surface hydroxyl groups with low density, leading to effortless diffusion and reduced aggregation. Incorporating HNTs and GnPs nanofillers into epoxy matrix composites produces a positive effect on the plasticity, mechanical strength, heat resistance, and longevity of the material. Further investigation is needed to determine the individual impacts of HNTs and GnPs as separate nanofillers (36-39).

2. Biopolymers

The amazing flexibility of intelligent materials has revolutionized sustainable product development. The capability to respond to outside stimuli and also change with it their surroundings has made them desirable for applications in engineering, defense, medicine, and automobile manufacturing. Memory alloys, hydrogels, pigments with color changing with light or temperature, and polymers which can recall and return to their initial form are examples of smart materials (40). Smart materials provide a major benefit in that they can be personalized to fit a certain usage, leading to a diverse array of physical, chemical, and biological attributes. The trend has presented engineers as well as researchers with stimulating opportunities to produce sophisticated single and combined systems that adjust to industry requirements. The development of science and engineering has resulted in a need for extremely innovative and environment-friendly materials which meet the requirements of contemporary industries. Engineers specialized in materials are always exploring methods to

utilize the distinct features of intelligent materials in an attempt to develop environmentally friendly and inventive goods which fulfill the demands of contemporary society (41). Heavy construction materials, in particular in transportation, are costly and call for a higher energy level, which produces considerable problems in the materials industry for handling and production. This has led scientists to research simple and cost-effective ways of producing lightweight and strong mechanically-absorbing polymer composites. Additionally, because green waste is lowering and carbon emissions rising, biopolymers are now being redesigned to enhance their properties and properties. Research into different biopolymers including Polylactic acid (PLA), polyhydroxyalkanoates (PHA) (42) starch, cellulose, pectin as well as chitosan has produced a selection of biopolymers and bio composites which share qualities with standard bio-packaging (43). Lightweight biopolymer composites should see automobiles dropping in weight by 50% within the next ten years, meaning a 50% decrease in gas use. The features of polymer composites and polymer-based ceramics might be utilized to develop as well as make innovative lightweight engines. Natural biopolymers possess many benefits, including their deliberate formation inside living organisms, their mixed properties in solid, semi-solid, and liquid forms, and their potential to be used with no further treatment, which is creating growing interest. In addition to that, they enable the easy development of thin coatings on solid surfaces, which happens to be a method of industries like printing arts, textiles, and packaging components (1,2). The surfaces are made more water-repellent and water-attracting by this technique. Contact lens surface enhancement has been discovered by utilizing cross-linked hydrogel coatings (44,45). Written works are examined principally as carbon-based polymers (nanoscale fibers & dispersions, cyclic fullerenes) and polymers made of boron and silicon. This particular thesis has emphasized biopolymers such as cellulose and its variations, such as Nitrocellulose, hydroxyethyl cellulose, carboxymethyl cellulose, along with oxycellulose. In (Figure 1) we see cellulose placed like a linear polysaccharide of glucose (46) which offers mechanical support for plant life, algae, fungi, and bacteria. Probably the most abundant and renewable resource on earth is cellulose, an all-natural polymer. The annual production of cellulose is thought to be 75 to 100 billion tons (3) (A number which has developed since 1912). It's generally obtained as pulp or extracted from organic sources such as cotton, bark, wood, jute, leaves, and timber. As a derivative of cellulose, CMC received significance for commerce and industry during the 1920s because of its easy production procedure as well as cost-efficient parts. CMC finds application in different industries including food, beauty products, pharmaceuticals, paper & textiles. Much like cellulose, the substance derivative nitrocellulose (NC) is commonly used in industries like coatings, varnishing, filtration membranes, printing inks, and numerous other purposes. Its particular nitrogen-based content (5,7,47) determines its useability for various uses. The creation of NC aerogel is growing its usage in purification science, separations, and biomedical applications (48). Oxycellulose (OC) is a non-toxic polymer that can degrade effortlessly over time to be employed in surgeries. it's suitable for living organisms and also may be utilized to avoid bleeding and tissue adhesion. The market provides the product in two forms - knitted fabric or staple fiber. HEC is a kind of cellulose that has no taste, is edible and has a strong water sensitivity. It's extensively used in the pharmaceutical, cosmetic, and food industries as depicted in (Figure 1.c) (11,12). HEC offers qualities including biocompatibility, biodegradability, and film-forming capabilities which cause it to be extremely appropriate to be utilized in biomedical methods (48). Food packaging materials are produced using aluminosilicates combined with natural biopolymers (49). This dissertation is designed to examine different biopolymers with a particular focus

on cellulose derivatives like hydroxyethyl cellulose as well as carboxymethyl cellulose. The biopolymers discussed previously are graphically shown in (Figure 1). The thesis will concentrate on the investigation of different polymer aspects including their spreading or diffusion, swelling phenomena, and breaking down operations, surface force, strength, and behavior of diffusion (50). The assessment (51-53) will focus on industrial additives employed in the printing as well as textile industries. These additives are utilized for several functions including safeguarding printing plates from dampness, protecting printing plates, and enhancing textile coloration. The areas of biopolymer cross-link-linking and diffusion coefficient will also be discussed. I will initially look at nanomaterials, polymers composites, polymer nano composites, and nanofillers, and any configurations of the polymers and its characteristics before proceeding to the characteristics of biopolymers.

3. Nanomaterials

Nanotechnology describes a scientific area and technological advancement wherein structures and devices are controlled as well as examined at incredibly small scales, including atomic, molecular, along with macromolecular levels. Scales generally measure between 1 to 100 nanometers (54). The word "nanotechnology" is believed to have its origins in (Japan), where Taniguchi (55) coined it. The importance of dimensions of roughly 1 billionth of a meter is particularly dealt with in this specific branch of manufacturing. Nanoparticles have been found to have advantages over bigger than microspheres as demonstrated by research (56). In addition, biological nanoparticles have mainly been created for drug delivery purposes as an alternative to liposome technology (57). The objective of this particular method is to tackle worries regarding the durability of liposomes in biological fluids while being kept. Nanoparticle technology is a brand-new advancement that could boost the effectiveness of medication. Colloidal drug delivery methods could include nanoparticles, therefore enabling modified body distribution for specific drug delivery (58). Additionally, they might improve the absorption of compounds into cells (59), which decreases the harmful and negative consequences of unbound medicines (60). Nanoparticles may be carried from the bloodstream to several locations within the entire body, facilitating treatments that target the whole system (61). It's possible to produce nanoparticles utilizing different materials including proteins and artificial polymers. The selection of materials for nanoparticles is determined by numerous elements, including their size and structure, area charge, flexibility, compatibility and biodegradability with living organisms, possible toxicity, and preferred drug release profile (62,63).

4. Biopolymer nanoparticles

For The first time, albumin (64) and non-biodegradable artificial polymers like polyacrylamide and poly (methyl acrylate) were utilized to develop biopolymer nanoparticles (65,66). The danger of extended harm resulting from the build-up of biodegradable polymers inside cells or tissues has become a significant obstacle to their application as a systemic therapy for human beings. The main focus was moved to nanoparticles created from man-made bio-degradable polymers including poly alkyl cyanoacrylate, poly (lactic-co-glycolic acid) and polyanhydride (67-70). The literature presents substantial exploration from several directions (71-76) on possible therapeutic uses of biodegradable colloid systems. Nevertheless, earlier studies (77,78) have cautioned these systems might encounter toxicological difficulties. Additionally, the hydrophobic qualities of the polymers utilized in

bio nanoparticle-based delivery methods exert a constraint on effectiveness in supplying hydrophilic substances like nucleic acids, proteins, and peptides (such as genes and oligonucleotides). The process of enclosing and shielding the drug against enzyme breakdown could be inefficient (75-79). Thus, scientists have looked at using naturally occurring materials that possess a greater water affinity for nanoparticle manufacturing (80-82). It had been recognized several years back those biodegradable nanoparticles are necessary for their usage as drug carriers (83). Liposomes, virus-like particles (VLPs), in addition to proteins, are biopolymer nanoparticles that possess a variety of benefits, including their simplicity of generating from obviously degradable polymers and their enhanced stability in natural fluids and storage (84). A report (85.) proposes that proteins and polysaccharides might be blended to make biodegradable nanoparticles that may deliver standardized, sustained, and targeted drugs. This delivery technique has demonstrated promising accomplishments in improving the therapeutic effects of drugs while lessening their negative effects.

5. Polymer composite and nanocomposite

PMCs and PNCs (Polymer composite & nanocomposite) consist of a Polymer element and additives including inorganic fillers which improve the structure and also the function when used. Or alternatively, polymer nanocomposites (PNCs) include molecules and fibers/films which measure somewhere between 5 and 100 nanometers in dimension, with no less than 1 nm of those elements contained. PCMs and PNCs are made and formed by utilizing both synthetic and natural polymers as matrices. The thermoplastic materials used in these methods can undergo reversible viscous flow upon heating or a curing agent when exposed to heat or a curing agent. Harito and colleagues (86) concluded that polymer nanocomposites (PNCs) are matrices of polymer or copolymer-containing nanomaterials or even nanofillers. Fillers containing at least 1 dimension measuring between 1 and 50 nm are specified. PNCs have applications in electronics, structural, biomedicine, and optics. Hashim et al. pointed to polymer thin films as crucial to a range of technical uses, which include adhesives and coatings, and natural products. (87). Redondo and colleagues, based on (88), the existing research emphasis is on adjusting the attributes of materials in polymer nanocomposites by altering the size as well as the number of nanoparticles. Nevertheless, the difficulty is based on effectively dispersing PNCs films or coatings. The polymer structure has nanoscale particles but with increasing amounts of particles, dispersion becomes problematic because of their tendency to aggregate together. To handle this particular issue, nanoparticles may have chemically altered the surfaces to create a consistent dispersion. Complex and costly fabrication methods might be created, possibly due to this (89). The function of the interface between nanoparticles along with polymers is incredibly important in identifying the physical, chemical, and also mechanical engineering attributes of polymer nanocomposites. (90). In traditional polymer composites, a particular filler could affect other significant qualities by impacting their general quality. A rise in stiffness of materials which block or hold off flames can reduce durability, see-through ability, or mechanical characteristics. Individually tailored nanoparticles can possibly reverse or eliminate specific properties declining while concurrently improving numerous desirable advantages within nanoparticles. (91). My studies suggest that perlite mineral filler plays a crucial part in the thermal and mechanical properties of HDPE polymer nanocomposites. The Young's modulus progressively increased with better filler concentration; break elongation decreased. Perlite concentration of 15 wt.% exhibited a 37 wt.% increase in Young's modulus of elasticity compared to pure HDPE. The stress-strain curve (Figure 2) was utilized to analyze all these factors. Non-destructive vibration analysis (displacement transmissibility measurements) confirmed the improved stiffness in uniaxial tensile mechanical strength experiments, which revealed a change in the original peak frequency direction (position) towards higher degrees

of excitation. The toughness against fractures reduced with increasing perlite content, suggesting the fractures were much more likely to be brittle fracture. However, SEM pictures showed places in which the fractures had been ductile-indicating greater filler levels-after examination of the material. Perlite particles added stress concentration to the composite matrix. The increased filler concentration was related to a modest temperature rise which was linked with melting, suggesting a stronger link between the particles of filler and also the chains of the polymer. Another study investigated the structural characteristics of epoxy resin nanocomposites containing nanoscale graphene nanoplatelets (GnPs) along with halloysite nanotubes (HNTs) as fillers. The experiment found that the modulus of elasticity of Young was altered nonlinearly by the inclusion of GnPs fillers. The nanocomposites experienced greater ductility when the GnPs nanofiller was between 1 and 0 wt.%. The reason for this might be the movement between specific GnPs, nanoparticles that have been separated into the matrix. Nevertheless, once HNTs fillers have been included, Young's modulus of elasticity remained fairly consistent. The HNTs nanoparticles were caught inside the surrounding material during mechanical tests and their movement was severely limited. The SSC plot results (Figure 2) demonstrated that the more rigidity epoxy/HNTs nanocomposites had greater fracture stiffness values at reduced filler levels than the epoxy/GnPs nanocomposite. The GnPs filler does this mainly because of its gliding dissipative effect. Elongation at break dimensions demonstrates the special epoxy/GnPs nanocomposite combinations become more plastic and ductile as the GnPs filler quantity increases. epoxy/GnPs nanocomposites showed a lower indentation modulus than ethylene HNTs nanocomposites based on micro-hardness assessments. The very first one shows more mechanical dissipation (the friction from the GnPs filler during a glide is in excess than the epoxy/HNTs. The research utilized a non-destructive mechanical damping technique for forced oscillations at a reduced frequency of 2-3,200 Hz to determine mechanical qualities by locating the first resonance frequency peak. The verification of this effect has established the plasticization effect in epoxy/GnPs nanocomposites. The epoxy/HNTs nanocomposites had a considerably greater peak position for 1st resonance frequency than some other components, indicating superior overall performance. The incorporation of little fillers including carbon nanotubes, nitrocellulose and carbon graphene makes it easier to manage and enhance polymer nanocomposites (86).

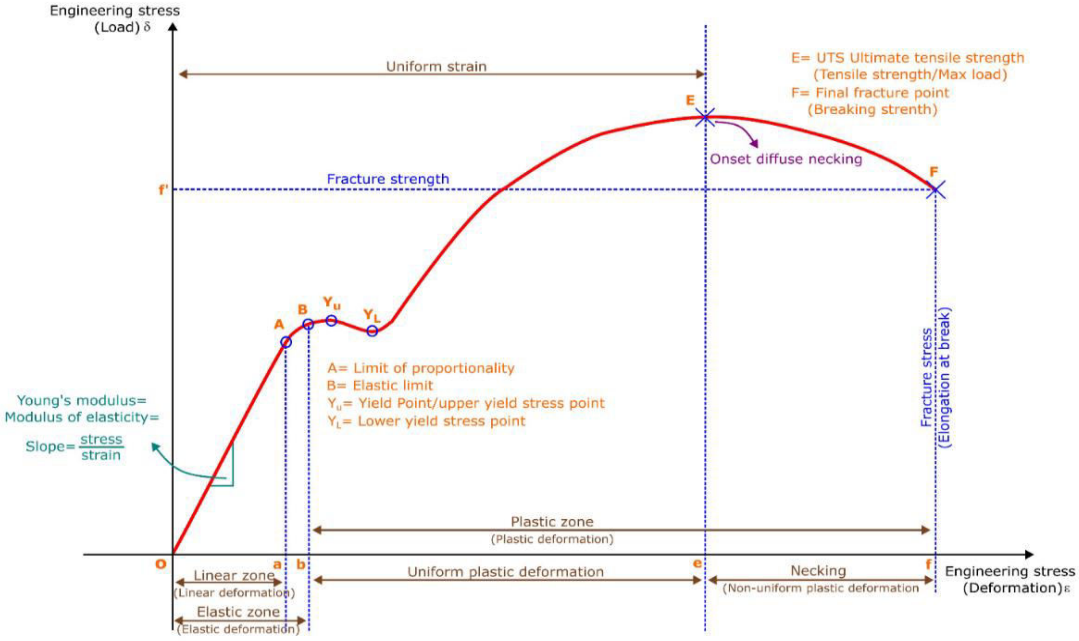

Figure 2. *A stress-strain curve (SSC).*

6. Nanofillers

Nanofillers, especially those made of clays and carbon nanotubes, have received a lot of attention in recent years. The widely accepted definition of nanoparticles requires that they have at least one measurement between 1 and 100 nm and that their remaining dimensions exceed 100 nm. It is feasible to classify these particles into more specific groups, depending on the number of dimensions they possess within the nanometer scale. Nanoparticles are zero-dimensional particles, nanofibers are one-dimensional particles, and nanoplates are two-dimensional particles. To begin with, it should be noted that nanofillers aren't a new concept; in fact, nanoparticle fillers are well-established on the market. The substances mentioned above consist of calcium carbonates, fumed and precipitated silicas, and carbon blacks. Synthetic polymer nanoparticles are also becoming popular. Our research studies investigate precisely how the mechanical and structural properties of HDPE composites, manufactured in a test facility, are influenced by the addition of nano-sized mineral fillers such as nano $CaCO_3$ and nano clay. The findings indicated that the inclusion of fillers had a notable positive impact on the mechanical properties of the composites. This was evident through an increase in both the elastic and indentation modulus. As an illustration, the HDPE's elasticity modulus rose by 51.5% to 1470.0 ± 54.7 MPa when 5% of nano $CaCO_3$ filler was added, and also by approximately 34.5% to 1304.9 ± 83.7 MPa when 4% of nanoclay filler was added. The type and amount of filler used in addition influenced the plastic-elastic mechanical properties of the materials. This was evident from the materials' decreased ability to stretch before breaking and increased area under the stress-strain curve at higher filler concentrations. The optimal filler concentration for both composite types was discovered to be 5%. Furthermore, the thermal stability of both nanocomposites was higher than that of pure HDPE, suggesting a far more robust bond with the HDPE matrix. These results indicate that the nanocomposites have the potential to be beneficial in complicated product designs as they possess both elastoplastic mechanical properties across a variety of deformation rates and increased stability in terms of heat. Although nanofillers have been receiving a great deal of attention lately, it is crucial to keep in mind that the concept is not new. Nanoparticulate material fillers have been on the market for quite some time and are widely recognized. Examples of these kinds of materials are carbon blacks, fumed silicas, and precipitated calcium carbonates. Thus, a significant portion of the potential nanoparticle market is currently content. The discovery is likely to manifest itself as nanoplates as well as nanofibers. In this specific context, nanoparticles are described as having at least one measurement that ranges from 1-100 nm, except for flat substances such as graphene that could potentially have a thickness smaller than one nm. In the absence of porosity effects, the particular surface area of the nanoparticles can range from 25 to much more than 750 m^2/g, which can be used to steer their movement. The mentioned trait is able to change depending on the specific weight and might display an unforeseen variation. When there is high density, a specific measurement decreases in its magnitude. Particles that have three dimensions at the nano scale are categorized as nanoparticles, whereas particles with one and two dimensions are known as nanofibers and nanoplates, respectively. This is depicted in (Figure 3).

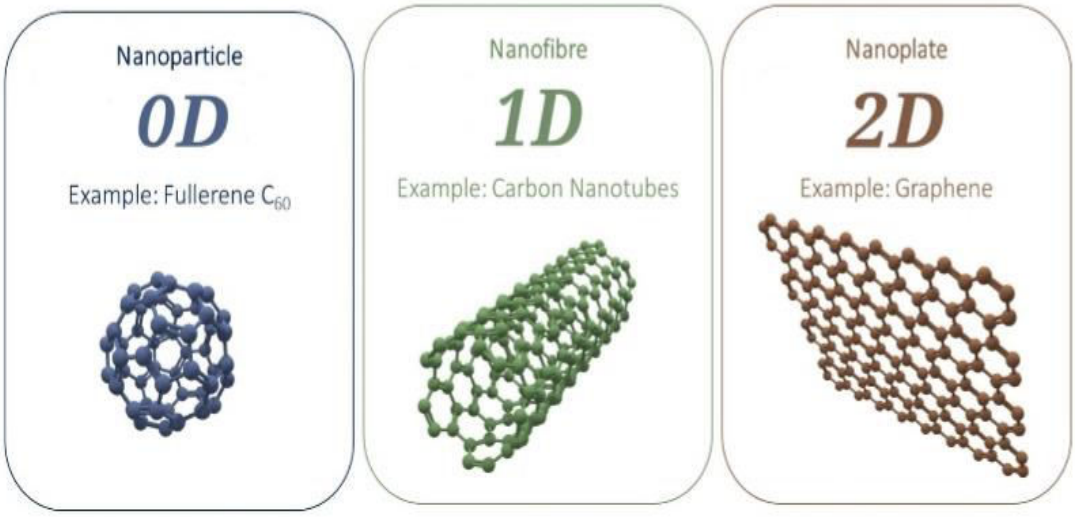

Figure 3. Nanoparticles, nanofibers, as well as nanoplates may be differentiated by the number of external measurements they possess on a nanoscale domain. Reproduced from (92).

7. Biological routes

Balaji et al. (93) highlighted the usage of natural substances as coating substitutes for enhancing the biocompatibility of polymers. In the latest analysis of covering techniques. A number of surface modification methods are continuously evolving to customize polymers' biocompatibility and improve their interaction with the natural environment which is usually known as biofunctionalization methods. The regular goal of these different techniques, discussed in detail and depicted in (Figure 4). It is adapting the surface qualities related to a certain polymer to direct its cellular interactions for the particular site where its application is focused. Though diverse biofunctionalization techniques are obtainable, the thought of utilizing natural materials for bettering biocompatibility appears effective and rational because of the biofriendly exterior in which they're offered that's closer to imitating the innate environment. Certain commonly found biomolecules, which include proteins, carbohydrates, and peptides, have gained popularity on valuable items through innovative methods.

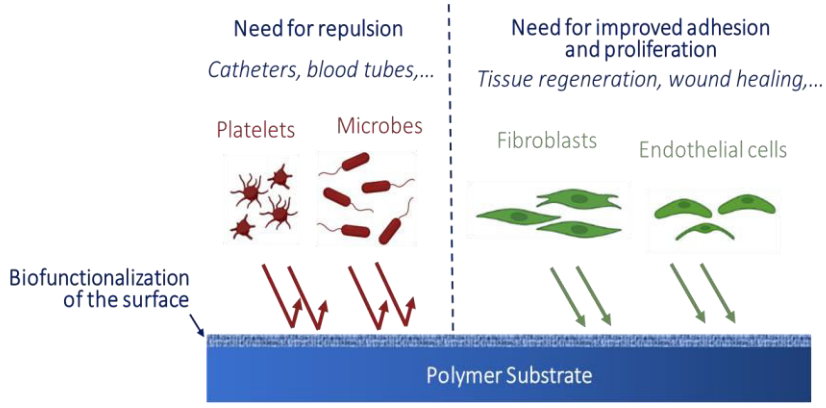

Figure 4. *The objective of biofunctionalization in relation to biomedical devices is to achieve specific goals. Reproduced from (93).*

According to current scientific studies, biological substances are attracting increasing scientific interest because of their nontoxic characteristics, compatibility with organic organisms, ability to replicate natural conditions, wide accessibility, and capability to prevent detrimental reactions related to synthetic polymer surfaces, like inflammation and also the adherence of platelets. Biomaterials applied to a surface might induce cellular attachment, development as well as specialization leading to an advantageous impact on wound healing and tissue regeneration. Biochemical methods entail the transfer of substances including lipids, medications, receptors, drugs, ligands, and peptides of proteins upon material surfaces through bodily adsorption, and chemical or self-cross-linking conjugation. Integrating environmentally friendly materials in biological techniques and eliminating damaging materials make them more appealing for enhancing the compatibility of polymers with living organisms. Surface chemistry is crucial for different biomedical applications because of its ability to adhere or react chemically, as is surface morphology like roughness or texture. There are situations where these requirements oppose one another for a specific material. The utilization of silicones in cardiovascular implants might require the promotion of advantageous cell attachment to facilitate the correct integration and connection of the synthetic unit at the implantation area. On the other hand, some catheter silicones might prevent cell adhesion to lessen contamination and blockage of the tube.

8. Properties of biopolymer

Biopolymers are polymers accessible naturally and are from living organisms. The source of a substance might distinguish between various classes including polyesters, nucleic acids, proteins, and carbohydrates. Biopolymers are appealing for different uses because of their diverse characteristics (ability to decompose effortlessly, compatibility with living organisms, replenishment, and long-term viability). Biopolymers are very appreciated for their capability to biodegrade, meaning they could be naturally decomposed by bacteria, and enzymes, together with various other all-natural mechanisms. Biopolymers are sustainable and may be utilized in areas involving reduced waste and pollution. Biopolymers aren't harmful and are compatible with living tissue or fluids. This distinctive property makes it ideal for biomedical uses like drug delivery methods and tissue engineering. Biopolymers tend to be inexhaustible and might be created by using sustainable energy sources like animals and plants, therefore permitting large-scale production without consuming natural resources. They are especially ideal for environmentally friendly and sustainably demanding applications because of this particular feature. Ultimately, biopolymers possess a different set of chemical and physical attributes which could be adjusted either by chemical alteration or by combining them with various polymers. For example, they possess great strength and durability, together with thermal stability, making them perfect for applications that require robust packaging materials together with some other uses where strength and longevity are essential. Biopolymers are appealing substances for different applications because of their assortment of distinct qualities, which include medicine, agriculture, packaging, along with various other sectors. While scientists continue to do research, they're finding new sources as well as strategies for creating biopolymers, which might have a wider utility scope.

9. Conclusion

The applications potential, natural breakdown, and distinctive characteristics of biopolymers have drawn significant interest in recent years across various industries. The dissertation examined several biopolymers (cellulose derivatives, starch, chitosan, and protein-based biopolymers). Biopolymers possess broader structures, slim films, and flexibility enabling a variety of smart uses. The evaluated biopolymers hold great possibility for constructing novel high-tech coatings for biomedical and non-biomedical applications. The biomedical uses of cellulose derivatives depend upon their lightweight features and compatibility with living organisms. Cross-linked starches are being studied for their unusual mechanical strength and water resistance. The dissertation thus gives a promising starting spot for scientists to investigate the uses of biopolymers in different areas. While biopolymers are analyzed a lot more profoundly, specialists are wanting to produce more advanced as well as substantial elements, opening the door for natural biopolymer coatings to far more closely correspond to the environment and operator requirements.

*****

10. Projects

10.1 Study of the material engineering properties of high-density poly(ethylene)/perlite nanocomposite materials

Our published research paper B focused on the effect of perlite mineral as being a nanofiller in polymer nanocomposites for exclusive needs. Re-search demonstrated that the thermal and mechanical characteristics of HDPE compounds had been considerably influenced by the perlite nanofiller concentration. An important finding was that Young 's modulus of elasticity increased as the amount of the filler increased. It means that the stiffness of the HDPE composites was improved with the inclusion of perlite. This outcome was backed by both destructive uniaxial tensile mechanical strength and also nondestructive vibrator mechanical dynamic testing, which measured via displacement transmissibility working with excitation forced oscillation damped a single-degree-of-freedom (SDOF) technique followed by thermal analysis as well. Nevertheless, the study as well observed a decreasing trend in fracture toughness strength as the perlite concentration increased. This implies that the presence of perlite resulted in a weak fracture (brittle fracture) conduct in the HDPE composites. Furthermore, SEM examination proved that ductile fracture processes occurred at climbing filler concentrations. This suggests that the composites exhibited both ductile and brittle fracture surfaces, based on the perlite concentration. Additionally, SEM imaging demonstrated that the filler particles and also polymer chains had comparatively strong bonds. This implies great interfacial interaction and also adhesion between the HDPE matrix as well as the perlite filler. Overall, the study demonstrated the substantial impact of perlite as a nano filler on the thermal and mechanical properties of HDPE composites, with improved stiffness along with an intricate fracture behavior (i.e., ductile and brittle) based on the perlite concentration. The solid bonding between the polymer chains as well as the filler particles further highlights the possibility for perlite to improve the functionality of polymer nanocomposites in specialized aims.

10.1.1 Materials

White pellets with lot number 1I19091333 of HDPE type 25055E on the Dow chemical company from (USA) have been utilized. The inorganic volcanic glass mineral perlite (Supreme Perlite Company, USA), with a d50 diameter of 447 nm along with a density of 1.10 g/m^3, continues to be used as filler particles (94). Perlite filler moisture content was 0.1 wt.%. 150 composite specimens of perlite/HDPE composites with inorganic filler percentages of five, ten, in addition to fifteen wt.% were made (dog bone design for tensile evaluation, Charpy's pendulum, and then damping dynamic vibrator examination). On the (German Arburg Allrounder) type 420 injection molding machine, composite specimens were made utilizing the injection molding technique. Applied processing temperature ranged from 190 to 220°C, mold temperature 30°C, injection pressure sixty MPa, and also injection rate 20 mm/s (95). Extrusion machine Scientific was used for composite and virgin samples extrusion at the handling ranging from 136 to 174°C, L/D = 40.

10.1.2 Methodology

10.1.2.1 Scanning electron microscopy

Images from an SEM were taken with a Hitachi SU 6600 (Japan) SEM. The Schottky cathode serves as the electron's origin. This microscope has a resolution in secondary electron mode (SE) of 1.3 nm and in backscattered electrons (BSE) of 3 nm. For these pictures, the SE and an accelerating voltage of 5 kV were employed. There was a 6 mm gap between the specimen and the sensor. Studied materials were placed on double-sided carbon tape on an aluminum holder.

10.1.2.2 Thermal analysis

Virgin HDPE thermogravimetry as well as DTA studies were carried out for perlite/HDPE nanocomposites using a concurrent DTA-TG device (Shimadzu DTG 60, Japan). Observations were made between 30 and 550°C at a heat flow rate of 10°C/min in an evolving nitrogen environment (50 ml/min). The crystallinity (wc) of the nanocomposites was calculated according to the Formula (1) (96,97):

$$W_C = \frac{\Delta H_m}{\Delta H_m^0} \times 100 \quad (1)$$

Here: ΔH_m^0 = 293 J/g is the heating of fusion for 100% crystalline material HDPE, warmed at a speed of 10°C/min (96-98), and ΔH_m J/g is calculated heat of fusion.

10.1.2.3 Uniaxial tensile testing

Injection-molded specimens had been mechanically tensile tried on a Zwick 1456 multifunctional tester (Germany). The measurements had been recognized according to CSN EN ISO 527 1 and CSN EN ISO 527 2 standards (99). Samples have been strained at ambient temperature up to fracture point at the test speeds of 50, 100, and 200 mm/min. Young 's modulus of elasticity and elongation at break happen to be computed from the stress strain correlations. Each experiment was repeated10 times at the surrounding temperature of 22°C, along with average values and standard faults have been calculated.

10.1.2.4 Charpy impact testing

With a fall energy of 25 J, impact testing was performed on the (German made) Zwick 513 pendulum impact tester according to CSN EN ISO 179 2 standards.

10.1.2.5 Displacement transmissibility measurement

The displacement transmissibility Td, that will be denoted through the system (100,101), talks about the component 's capability to control dynamic mechanical damped vibrations which is excited harmonically induced in single-degree-of-freedom systems:

$$T_d = \frac{y_2}{y_1} = \frac{a_2}{a_1}, \tag{2}$$

Where y_1 is the displacement capacity on the examined specimen input side and y_2 represents the displacement amplitude over the specimen output side, a_1 is the speed amplitude over the input side with the tested sample and a_2 is the acceleration amplitude over the output side with the examined sample. Based on the magnitude of the displacement transmissibility, there are generally 3 major types of dynamic vibrations: resonance ($T_d>1$), undamped ($T_d=1$), and as well damped $T_d(-)$ or ($T_d<1$) vibration (101). The consequent formula (3) (100-102) provides the displacement transmissibility of a spring mass damper process, that is represented through the spring 's stiffness (k), damper's damping coefficient (c), and the mass (m):

$$T_d = \sqrt{\frac{k^2+(c\times\omega)^2}{(k-m\times\omega^2)^2+(c\times\omega)^2}} = \sqrt{\frac{1+(2\zeta\times r)^2}{(1-r^2)^2+(2\zeta\times r)^2}} \tag{3}$$

Where exactly the coming equations (4) and (5) (103,104) are used to explain the damping proportion ζ along with the frequency proportion, respectively:

$$\zeta = \frac{c}{2\sqrt{k\times m}}, \tag{4}$$

$$r = \frac{\omega}{\omega_n} = \frac{\omega}{\sqrt{k/m}}, \tag{5}$$

where ω_n is the purely natural frequency plus would be the oscillation frequency (105,106), And finding the frequency ratio r_0 where displacement transmissibility reaches its greatest point (172) is possible if dT_d/d_r = zero in Equation (3):

$$r_0 = \frac{\sqrt{\sqrt{1+8\zeta^2}-1}}{2\zeta} \tag{6}$$

Formula (6) makes it very clear that with a much better damping ratio ζ the regional maximum of the displacement transmissibility is normally transferred to lower amounts because of the frequency ratio r (or with the reducing material stiffness k). The area extrema (i.e., Equation 6) results probably the highest amount with the displacement transmissibility

$T_{d(max)}$ in the frequency ratio r_0 . The forced oscillation technique was utilized to estimate the

values under investigation for dynamic vibration damping. At frequencies between 2 to 3,200 Hz, the Td was driven using the BK 4810 vibrator along with a BK 3560-B-030 signal pulse multi analyzer and also a BK 2706 power amplifier. Employing BK 4393 accelerometers (Brüel & Kjaer, Nrum, Denmark), the acceleration intensities (a_1 and a_2) on the input and output sides of the considered samples were measured 3 featured inertial masses of bandwidth 0, 90, and 500 g - that were set on top of the periodically evaluated specimens were used to define the displacement transmissibility. The studied block item dimensions were (60 × 60 × 3) mm (length × width × thickness). Each measurement was taking placed five times at a temperature of 23°C.

10.1.3 Results and discussion

As reported in earlier studies (99), inorganic nano/microparticles are used as functional fillers to alter the elastic plastic aspects of polymer composites. It was discovered that the key drivers of the adjusted react structures of these supplies tend to be the physicochemical attributes of the polymer matrix, LLDPE, LDPE, and HDPE alongside the properties of the filler particles (like morphology, diameter, shape, and functionalization of the surface chemistry). The ratio alongside the polymer matrix's amorphous to crystalline regions and the effectiveness of the interface adhesion between the filler molecules as well as the polymer matrix are two extra essential details which should be taken into our consideration (107). SEM pictures of the perlite micro/nano filler particles are showed below in (Figure 5a and 5b). The existence of

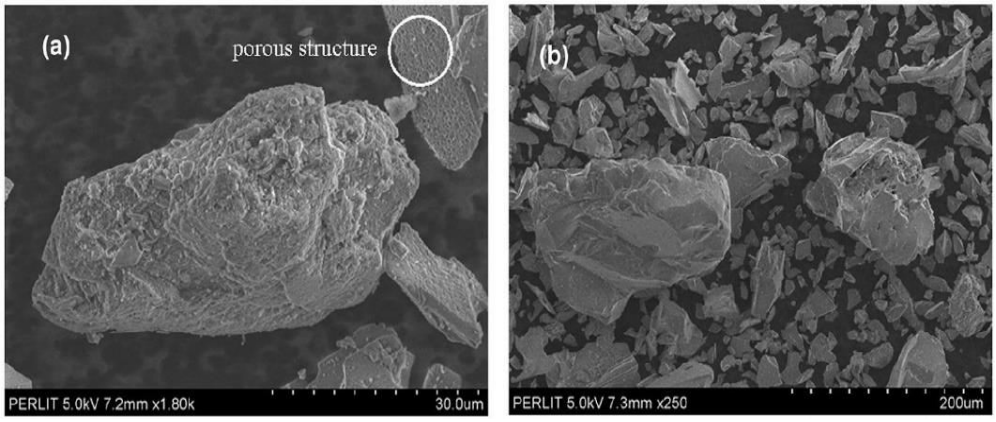

Figure 5. *The perlite micro/nano-filler is depicted in an SEM image.*

There is evidence confirming their permeable (porous) inner composition is supported by proof (Figure 5a). It is generally understood from a variety of sources (94,108,109) that the sound absorption, vibration damping, and dynamic mechanical characteristics of fillers or entire composites are directly influenced by their porous micro/nanostructures (95,110,111). The concentration of filler has a noticeable impact on the Young's modulus of elasticity (E) in the perlite/HDPE composites tested, as shown in (Figure 6).

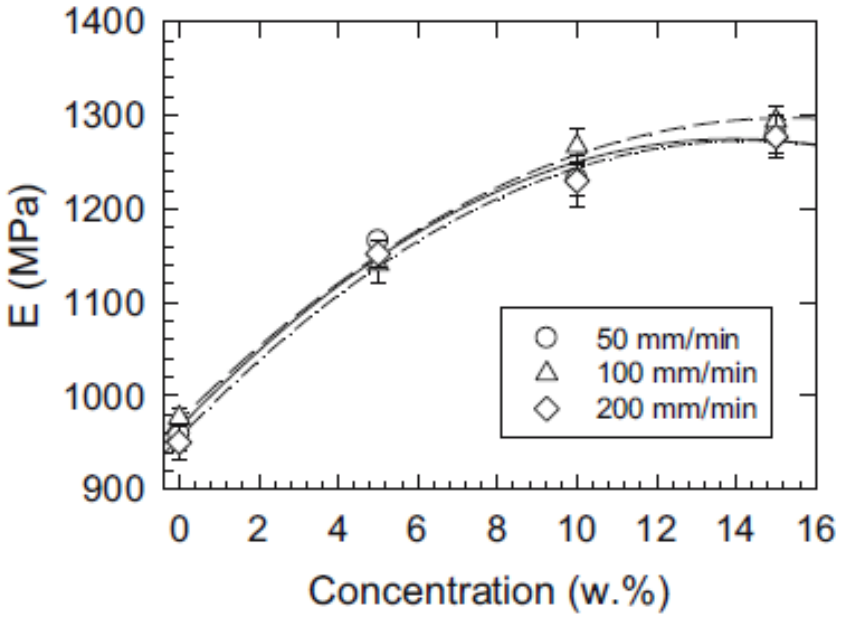

Figure 6. *The relationship between the concentration of inorganic perlite fillers and the modulus of elasticity (E) of Young's approach. Inset: Rates of deformation applied.*

The steady increase in E with greater perlite content was characterized by deformation rates of 50, 100 as well as 200 mm for all researches. A 37% increased E was observed for HDPE samples that contain 15 wt.% perlite, which is the same as the E value of pure HDPE. This led to a significant increase in the stiffness of the materials. As illustrated in (Figure 7), there had been a gradual decrease in the elongation at break observed with increasing filler content, following an exponential pattern.

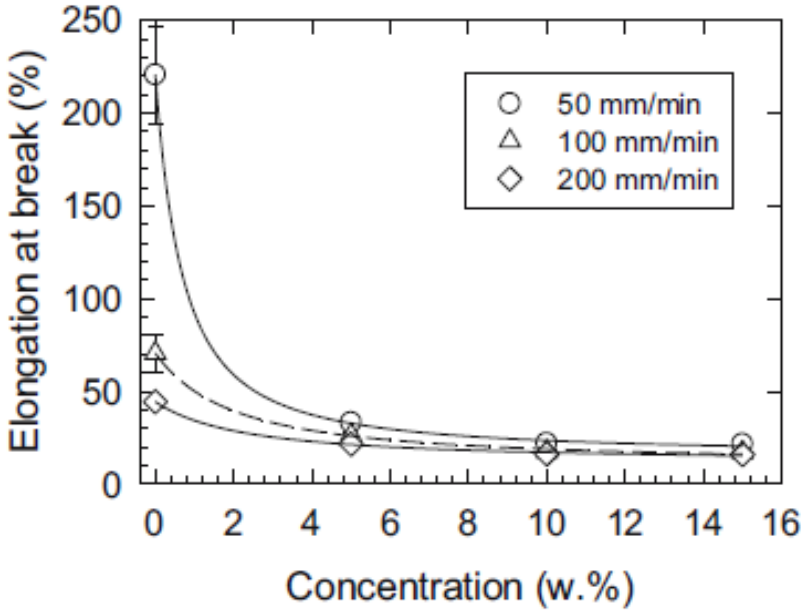

Figure 7*. Perlite filler concentration vs elongation at break. Inset: Rates of strains applied.*

The (Figure 8) indicated the consequences of fracture toughness evaluation was done.

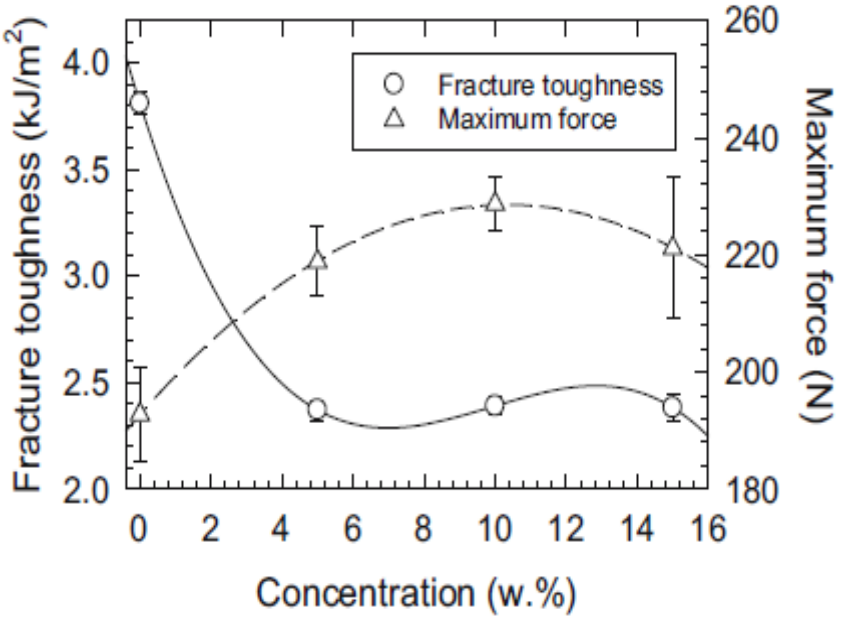

Figure 8. *The correlation between the concentration of inorganic perlite fillers as well as the maximum force and fracture toughness is interdependent.*

The fracture toughness of perlite/HDPE composites showed a substantial decrease, going from 3.8 kJ/m^2 (for pure HDPE) to 2.4 kJ/m^2 within the perlite concentration range of 5 to 15 wt.%. The addition of the mineral filler increased the stiffness of the composite material, as demonstrated during the previous uniaxial tensile testing. This was evident in the increasing modulus (E) as the concentration of filler increased. The Charpy pendulum was utilized to confirm the impact strength during the assessment of fracture (Figure 8) because of the rise in both the maximum force as well as the filler content concerning. The suggested mechanism for transferring mechanical energy, it is apparent from the scanning electron microscope pictures (Figure 9) that there are distinct areas of brittle fracture, as seen in (Figures 9a and 9b), as well as polymer regions that have undergone plastic deformation, characterized by the presence of spurs and deformation shear bands, which are typical of ductile fracture interfaces.

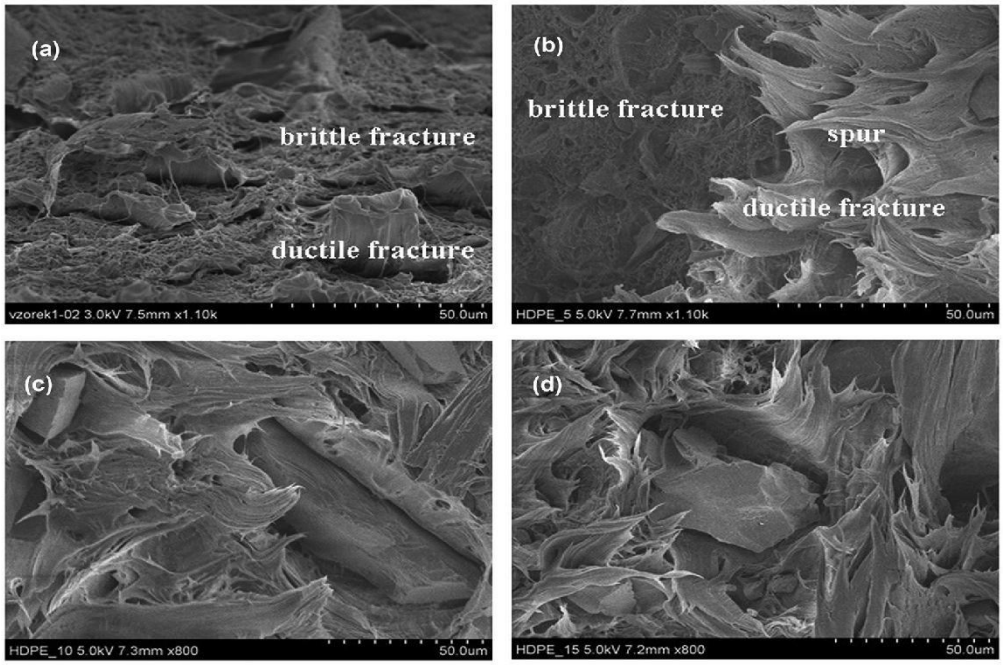

Figure 9. *Scanning electron microscope (SEM) images of the fractured surface were observed after conducting mechanical tensile tests on the samples. HDPE composites with perlite content of 5%, 10%, along with 15% by weight. (Applied deformation rate: (50 mm/min).*

The investigation of the frequency's correlation to the displacement transmissibility which was used to determine the dynamic mechanical vibrations aspects of the composite materials being undergone the examination are displayed in (Figures 10 as well as 11).

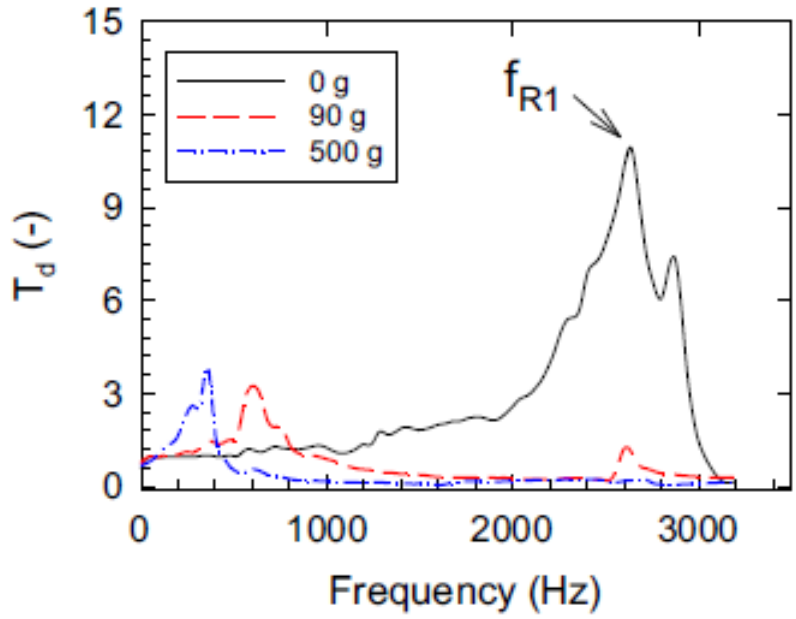

Figure 10. *Relationship between displacement transmission frequency and tested perlite/HDPE composites). The concentration of perlite without any inertial mass is zero.*

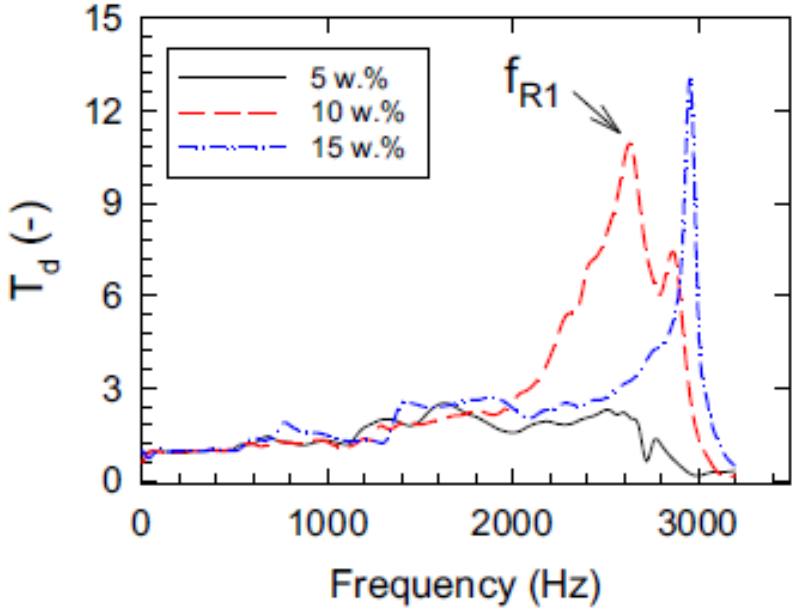

Figure 11. *The displacement transmissibility of the perlite/HDPE polymer nanocomposites under examination was frequency dependent. The inertial mass contains 10 weight percent of perlite.*

The position of the first resonance frequency peak (f_{R1}) in (Table 1) suggests that there is increased stiffness in materials with higher filler concentrations. This is in line with the displacement transmissibility frequency patterns revealed in (Figures 10 as well as 11).

c [wt%]	Quantity	Inertial mass (g)		
		0	90	500
5	f_{R1} [Hz]	1,614 ± 72	593 ± 26	341 ± 15
	T_{dmax} [–]	2.5 ± 0.2	3.1 ± 0.2	3.7 ± 0.3
10	f_{R1} [Hz]	2,627 ± 112	603 ± 25	346 ± 16
	T_{dmax} [–]	12.1 ± 0.9	3.3 ± 0.2	4.5 ± 0.4
15	f_{R1} [Hz]	2,944 ± 129	626 ± 28	396 ± 17
	T_{dmax} [–]	14.2 ± 1.1	4.6 ± 0.3	4.8 ± 0.4

Table 1. *The composites that were examined were subjected to harmonically induced vibrations in order to ascertain their initial resonance frequency, f_{R1}, and their maximum displacement transmissibility, $Td_{(max)}$, that could be accommodated. the concentration of c-perlite.*

Equation (6) was evaluated for accuracy, and the results demonstrated that the f_{R1} peak position moves towards higher excitation frequencies as stiffness increases (or damping ratio decreases). The results of the mechanical tensile testing, which included measuring the concentration of perlite within the polymer composite matrix, were in complete agreement with the resulting dynamic mechanical vibrations behavior, while conducting vibrational tests, it was noticed that an increase in inertial mass caused a shift of f_{R1} towards lower frequencies of excitation harmonically. The observation that the normal frequency decreases with an increase in inertial mass (m) is supported by Equation (4), which in turn results in a alongside decrease in f_{R1}. Vibration damping method enables the evaluation of stiffness of polymer nanocomposites without causing any harm or destructive, unlike the damaging or destructive tensile or fracture assessments. The thermal analyses are presented in (Table 2) and (Figure 12).

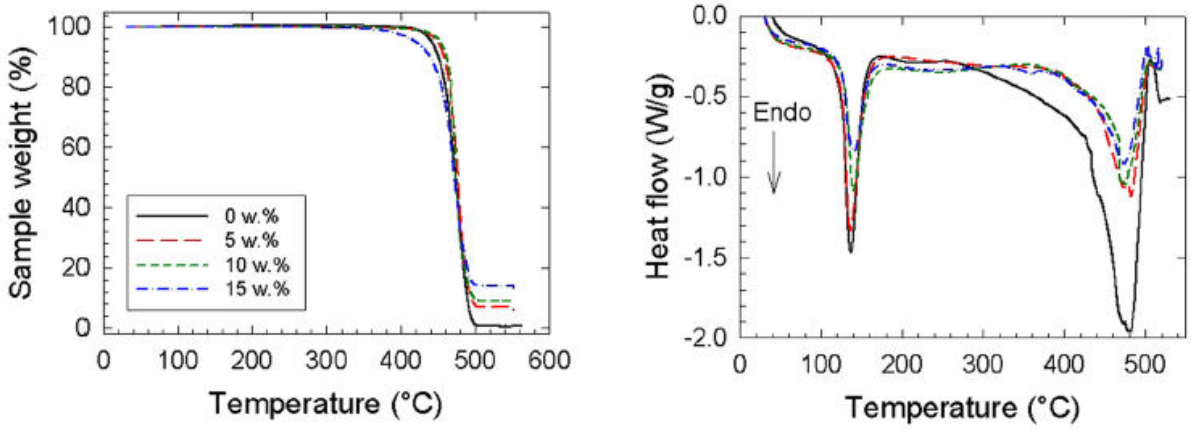

Figure 12. *The TG-DTA thermal examination results for the perlite/HDPE polymer nanocomposites have been determined. Inset: Concentration of perlite.*

c [wt%]	T_m [°C]	ΔH_m [J g^{-1}]	w_C [%]	T_A [°C]	T_D [°C]	TWL [%]
0	137.4	177.7	60.65	455	477.2	100.0
5	136.4	133.9	48.10	463.9	476.1	93.1
10	139.9	92.9	31.44	462.1	474.7	90.0
15	141.6	82.5	28.59	451.3	474.3	86.2

Table 2. *The study examined the thermal properties of both pure HDPE and polymer nanocomposites made with perlite and HDPE. The analysis focused on a number of parameters including the concentration of filler (c), the melting peak point (T_m), the temperature of fusion (H_m), the crystallinity (W_C), the peak of fission in the (DTA) curve (T_D), the initial point (T_A), the total weight loss (TWL), and the endothermic course of action for Hm for each specimen. The temperature range for the analysis was between 95 and 175 degrees.*

10.1.4 Conclusion

The study investigated the influence of perlite mineral filler on the mechanical and thermal properties of HDPE polymer nanocomposites. The findings demonstrated that as filler content increased, Young's modulus of elasticity gradually rose with the decline in elongation at break. At 15 wt.% perlite concentrations, there was a 37% increase in Young's modulus of elasticity compared to the virgin HDPE. Nondestructive dynamic mechanical vibrator testing confirmed the increased stiffness, as indicated by the shift of the first resonance frequency peak position to higher excitation frequencies. However, the fracture toughness showed a decreasing trend with increasing perlite concentration, suggesting brittle fracture occurrence. Regions of ductile fracture processes were observed at higher filler concentrations through SEM images, which were characterized by polymer deformation shear bands and spurs. In the complicated composite matrix, the perlite particles behaved as stress concentrators The research also discovered a little rise in melting temperature with rising filler concentration, suggesting a more solid link between the polymer chains and the filler particles. Ultimately, the findings imply that the thermal and mechanical characteristics of HDPE polymer nanocomposites are considerably influenced by the perlite mineral filler.

*****

10.2 Enhancement of the mechanical properties of HDPE mineral nanocomposites by filler particles modulation of the matrix plastic/elastic behavior

Research paper C investigates the use of two separate mineral fillers at the nanoscale level (nano clay and nano calcium carbonate) in the production of HDPE materials. The composites that were created were analyzed for their physical and mechanical characteristics. Making use of various techniques such as scanning electron microscopy, transmission electron microscopy, along with energy dispersive spectroscopy, the scientists confirmed that the fillers in the tested samples were evenly distributed. According to the study, the addition of fillers enhanced the mechanical characteristics of polymer composites. Due to the inclusion of additional fillers, there was an increase in both the elastic modulus as well as the indentation modulus. The final composites plastic-elastic mechanical performance was affected by the filler type and concentration used. In summary, the research indicates that incorporating nanosized mineral fillers, like nano calcium carbonate and nano clay, can enhance the physio-chemical characteristics of HDPE composites. The specific impact varies based on the type and amount of filler used.

10.2.1 Materials

The material utilized in our study was HDPE of HD8100M quality, which was obtained from polymer marketing company limited in (Thailand). The density measurement was 0.952 grams per cubic centimeter, while the melt flow index was 0.25 grams per 10 minutes. The nano calcium carbonate particles referred to as adaCAL-N1-C were procured from Adacal co. located in (Turkey) and underwent stearic acid treatment prior to being processed. The scanning electron microscopy (SEM) confirmed that the particles had an average size of 0.05 m. The nano clay particles, specifically EsanNANO 1-140, were provided by Eczacbas Esan in (Turkey) and their average size was determined to be 2.7 μm through laser diffractometer measurements. The uniform distribution of nanofillers within the HDPE matrix was verified by TEM and SEM pictures (Figure 13), and this was additionally supported by EDS mapping.

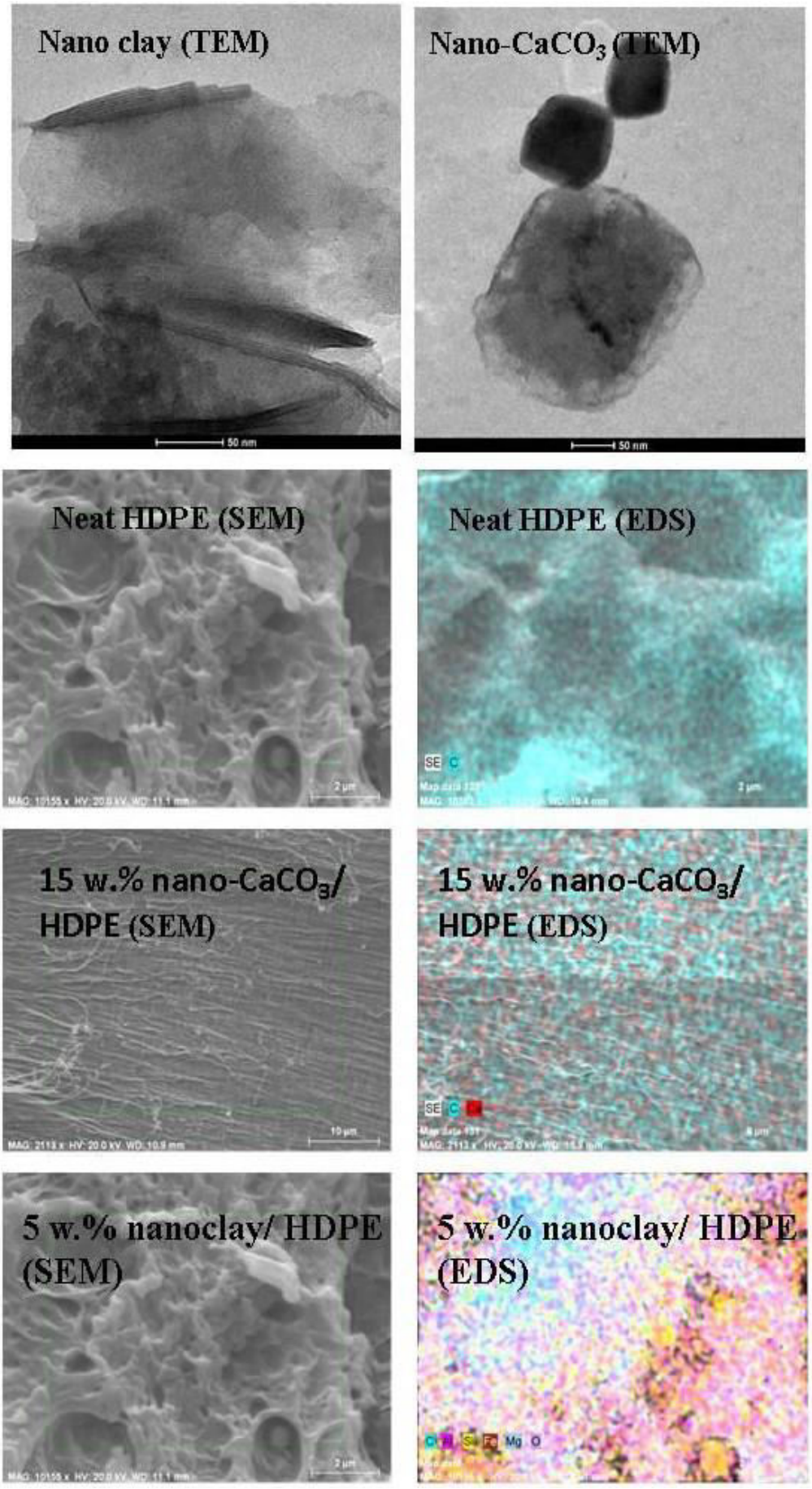

Figure 13. *This research utilized inorganic nanofillers that were pictured on TEM. Nano clay as well as nano calcium carbonate are additionally found.*

The chemical and physical features of the fillers are given in (Table 3) and are available in refs (112,113).

Filler type	Color	Density (g/cm^3)	Surface area (g/m^2)	Particle size (µm)
Nano clay	Highly white	1.98	19	2 – 20
Nano-$CaCO_3$	Highly white	2.95	28	0.05 – 0.10

Table 3. *Application of inorganic fillers and physical properties. Nano clay and nano calcium carbonate are additionally examined.*

Various filler concentrations have been arranged and categorized as CC for nano calcium carbonate and also NC for nano clay. A process was conducted to combine nano clay and HDPE, as well as nano calcium carbonate and HDPE, to create nanocomposites. This was done utilizing a melt blending system that included a Banbury blender, one screw extruder, along with a granule cutting unit. The production rate was 100 kg. The mixer contained a combination of HDPE granules and also filler, and also the temperature for processing was maintained at 180°C, which was attained in 15 minutes (114). The extruder screw speed was 330 rpm, and it had a temperature profile consisting of five-barrel temperatures: 200, 190, 190, 190, and 220°C. Afterwards, the nanocomposite blends were separated into small pellets and utilized as experimental specimens for conducting tensile and also impact assessments. To obtain the desired results, the PS40E5ASE injection molding equipment was utilized. The equipment had a melt temperature of 210°C, mold temperature of 65°C, and injection pressure of 50 MPa. The wetting liquids used for measuring contact angle were Millipore water from the (USA), which had a conductivity of 0.06 µs/cm, ethylene glycol p.a. from Lach-Ner in (Czechia), and 99% pure diiodomethane of ACS reagent degree from Sigma Aldrich.

10.2.2 Methodology

10.2.2.1 SEM and TEM

To determine the structure among with morphology of the filler particles, TEM (FEI Tecnai G2 Spirit Biotwin model, FEI Company, USA) was employed. The nanofiller specimens were deposited onto a standard 400-grid copper mesh and subsequently scattered in acetone via ultrasonication for 15 minutes. The dispersions were then cast on the copper mesh and air-dried. TEM measurements were conducted at an accelerating voltage of 120 kV. The distribution of nano $CaCO_3$ and nano clay in the HDPE matrix was analyzed by TEM, wherein an ultra-thin section of approximately 100 nm thickness was obtained from the filled samples using a microtome device (CM1950) from Leica Microsystems Inc. (Buffalo Grove, USA) in a low-temperature environment. To conduct a more comprehensive analysis of the nanofiller distribution, the composites underwent SEM characterization utilizing a (Zeiss EvoLS10) instrument via an energy-dispersive X-ray detector (Germany).

10.2.2.2 Thermal analysis

Differential Scanning Calorimetry (DSC) evaluations were conducted in accordance with ASTM E1356, utilizing a TA Instrument S10 model (Waters, USA) under a nitrogen flow rate of 50 mL/min. The glass transition temperatures (T_g) of both virgin HDPE, as well as its

nanocomposites, were ascertained through DSC curves utilizing the midpoint method at a heating rate of 10°C/min from 30 to 300°C (113-115).

10.2.2.3 Uniaxial tensile testing

Tensile testing of injection-molded specimens was conducted using a universal testing machine autograph AGS-100 Shimadzu from (Japan) and a Zwick 1456 multipurpose tester from (Germany) equipped with a compact thermostatic chamber TCE Series. The data was collected following the CSN EN ISO 527-1 and CSN EN ISO 527-2 norms, utilizing an assessed gauge length of 8 cm. The experiments were carried out at room temperature with deformation rates of 50, 100, and 200 mm/min until the specimens broke. The stress-strain dependence plot was used to obtain the strength at break, Young's modulus, and strain at break. Each study was conducted again 10 times, and the mean values along with standard deviation were computed. The experiments were conducted under laboratory ambient conditions at a temperature of 25°C.

10.2.2.4 Charpy impact testing

The impact tests were conducted by dropping a 25 J energy pendulum using a Zwick 513 Pendulum Impact Tester (Germany) following the CSN EN ISO 179-2 standard. The experiments were repeated 10 times to obtain mean values and standard deviations.

10.2.2.5 Surface free energy (SFE) characterization

The surface free energy (SFE) of both pure HDPE and the researched composites was determined using axisymmetric drop shape assessment, with measurements of the static contact angle of wetting. The measurements were conducted at 23°C using a Krüss DSA 30 (Krüss, Germany), and repeated seven times. To determine the SFE, Owens, Wendt, Rabel, and Kaelble's extension of Fowkes's theory was utilized, which relied on the average static contact angles for water, ethylene glycol, and diiodomethane (116,117).

10.2.2.6 Microhardness

The micro-indentation exams were taken place using a micro combi tester (Anton Paar, Austria) due to the CSN EN ISO 14577 standard. A diamond tip of a cube corner shape (Vickers, Anton Paar, Austria) was used for the measurements. The loading rate (unloading rate) was set at 6 N/min, the maximum load was 3 N, and there was 90s holding time. The depth-sensing indentation procedure was employed for the concurrent measurement of the force on the indentor and the displacement of the indentor's tip. The placement of the indentation hardness (H_{IT}) was studied by carrying out a division of the maximum load (F_{max}) by the projected region of the hardness impression (A_p). The indentation modulus (E_{IT}) was computed by estimating the Poisson's ratio (ν) of the specimens (0.3–0.4) (118,119)) and using the plane strain modulus of elasticity (E*).

$$H_{IT} = \frac{F_{max}}{A_p}, \tag{7}$$

$$E_{IT} = E^{\star}(1 - \nu^2). \tag{8}$$

After conducting the measurements 10 times, the average values and deviations were calculated. The experiments were carried out in a laboratory setting at a temperature of 25°C.

10.2.3 Results and discussion

The findings from the experiments conducted on the composites were condensed in (Figure 14). The obtained deformation curves for stress versus strain displayed the typical patterns of elasticity (up to a 3% strain for minor deformations), a region where elasticity switches to plasticity (up to a 10% strain for minor deformations), in addition to a region where stress remains constant. The above-mentioned occurrence was noticed in composites of HDPE with 5 wt.% nano clay and 15 wt.% CC, when exposed to strains greater than 18% and 12%, respectively. This observation was reported in reference (120). The curves seen in this particular study were comparable to those found in our earlier research on mineral composites of industrial HDPE under the exact same deformation rate (113-115). Additionally, investigations were conducted on industrial HDPE mineral composites of industrial HDPE under the same deformation rate (185-187). When there was no stress plateau-draw area, the tensile deformation behavior of pure HDPE was more rigid. On the other hand, the 1 wt.% filler concentration in CC/HDPE composites exhibited a greater degree of elastoplastic behavior, as shown in (Figure 14b).

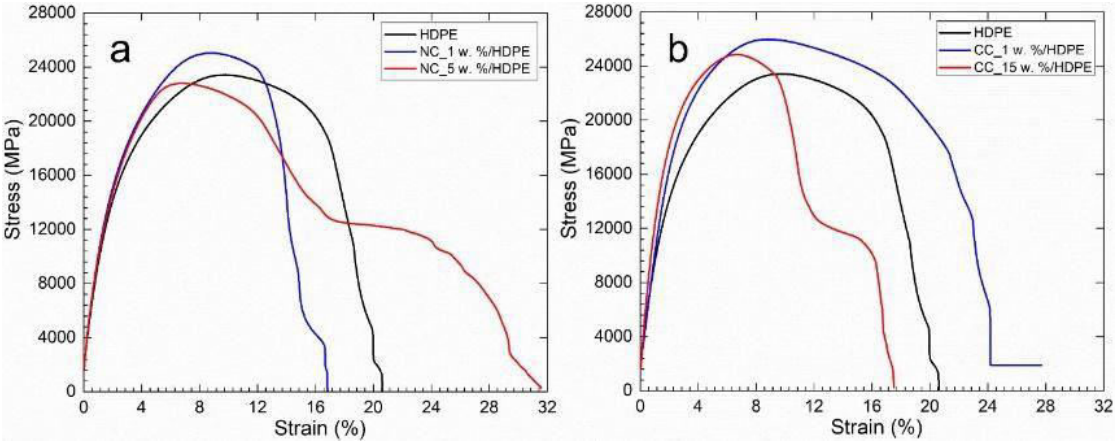

Figure 14. *(a) The overall mechanical performance of NC/HDPE, as well as (b)CC/HDPE composites, was examined by conducting tensile tests at room temperature, with a constant deformation rate of 50 mm/min, while varying the concentration of fillers. The outcomes are displayed as dependencies between strain and stress.*

The behavior of NC/HDPE composites was significantly influenced by the elastic-plastic characteristics. Increasing the concentration of fillers led to improved plastic behavior, as shown in (Figure 15).

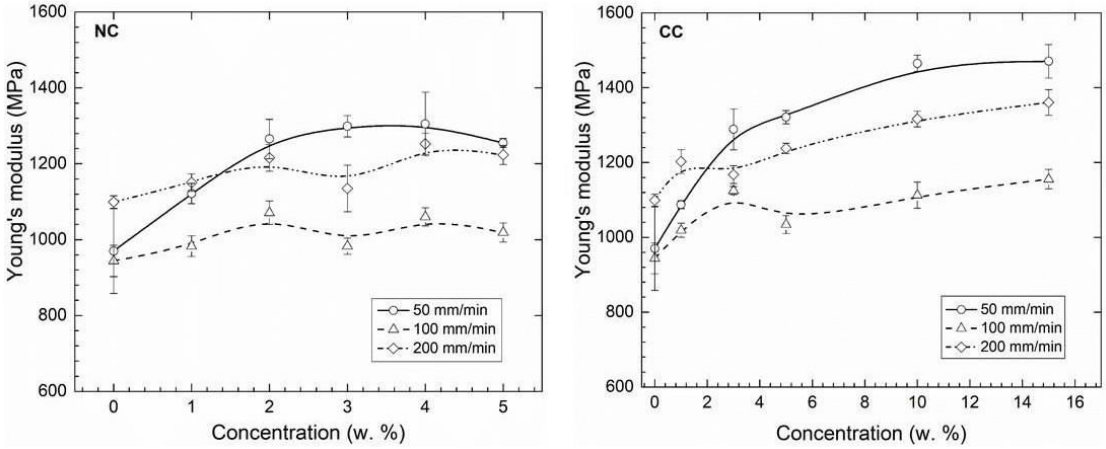

Figure 15. *The relationship between Young's modulus and the amount of filler present in CC/HDPE and NC/HDPE composites was investigated by conducting tensile tests at various deformation.*

This behavior was seen in all rates of deformation as shown in (Table 4). To illustrate, the CC/HDPE composites containing 5 wt.% filler concentrations experienced an increase of approximately 51.5% in the modulus of elasticity from the original HDPE's absolute rate of 970.1 ± 111.7 MPa to 1470.0 ± 54.7 MPa. The addition of 4 wt.% inorganic filler levels resulted in a 34.5% increase in the modulus of elasticity for the NC/HDPE composites, achieving an absolute value of 1304.9 ± 83.7 MPa. The results are consistent with prior data, indicating that the gradual increase in the elasticity modulus of polymer composites as the filler content increases (121,122) may be due to the presence of rigid mineral filler particles.

Sample	Young Modulus (MPa)			Upper Yield (MPa)			Strain at Break (%)			Fracture Toughness (kJ/m^2)
	Rate (mm/min)			Rate (mm/min)			Rate (mm/min)			
	50	100	200	50	100	200	50	100	200	
HDPE	970.1 ± 111.7	943.8 ± 142.2	1099.2 ± 16.2	24.5 ± 1.1	24.8 ± 1.1	25.6 ± 0.4	20.5 ± 0.1	25.8 ± 5.0	16.6 ± 0.6	36.69 ± 5.15
CC_1%	837.5 ± 10.8	648.2 ± 419	1202.7 ± 32.1	25.4± 0.6	24.3 ± 1.1	25.1 ± 0.5	30.8 ± 3.1	33.2 ± 6.7	19.8 ± 0.3	31.48 ± 2.43
CC_3%	1288.9 ± 54.7	1368 ± 2.5	1167.7 ± 23.7	24.4 ± 0.4	25.0 ± 0.2	24.7 ± 0.8	22.0 ± 0.8	19.8 ± 1.0	22.9 ± 1.5	17.26 ± 0.92
CC_5%	1322 ± 10.8	1034.3 ± 299	1237.9 ± 13.7	23.6 ± 0.5	25.4 ± 3.4	25.0 ± 1.1	25.0 ± 3.0	28.5 ± 14.7	17.2 ± 3.1	26.29 ± 1.04
CC_10%	1465.1 ± 12.3	1112.8 ± 273	1316.4 ± 0.4	24.3 ± 1.3	25.2 ± 1.0	26.3 ± 0.7	18.6 ± 2.3	20.5 ± 7.4	14.1 ± 0.4	28.69± 3.4
CC_15%	1470 ± 54.7	1155 ± 255	1360.7 ± 1.7	24.6 ± 0.2	25.3 ± 1.1	28.1 ± 2.8	20.1 ± 2.6	19.7 ± 6.9	11.2 ± 2.2	31.79 ± 3.94
NC_1%	1121.4 ± 26.8	982.9 ± 217	1150.5 ± 23.0	23.6 ± 1.5	26.5 ± 0.5	27.4 ± 2.4	32.8 ± 15.9	19.3 ± 4.6	16.4 ± 6.0	29.21 ± 2.21
NC_2%	1265.4 ± 51.9	1070.9 ± 303	1215.6 ± 48.8	25.8 ± 3.2	27.4 ± 2.2	30.0 ± 2.8	21.2 ± 8.7	20.5 ± 10.5	12.1 ± 0.6	24.37 ± 1.0
NC_3%	1248.7 ± 28.1	982.7 ± 213	1134.9 ± 61.2	27.3 ± 1.9	23.9 ± 1.6	22.4 ± 0.4	19.8 ± 3.2	31.1 ± 11.2	26.6 ± 2.2	28.44 ± 0.09
NC_4%	1304.9 ± 83.7	1060.1 ± 240	1328.3 ± 78.0	23.3 ± 0.1	23.9 ± 0.3	27.9 ± 2.5	27.6 ± 2.2	35.7 ± 7.2	14.4 ± 5.9	23.35 ± 0.27
NC_5%	1255 ± 11.9	1018.8 ± 246	1223.3 ± 25.0	23 ± 0.2	23.5 ± 0.2	24.7 ± 0.2	28.9 ± 2.7	32.88 ± 10	20.5 ± 2.1	22.06 ± 1.42

Table 4. *The research study presents the results of testing the tensile properties of HDPE composites at three different deformation rates: 50, 100, and 200 mm/min. The sample description provides information about the concentrations of fillers, which are expressed as weight percentages.*

(Figure 16) illustrates that both nano clay and nano calcium carbonate fillers exhibit nonlinear patterns in terms of their upper yield and filler concentration dependencies in HDPE composites. Nonetheless, the upper yield of CC/HDPE composites did not exhibit notable alterations as the filler concentration increased, except for the composites that contained 4 and 5 wt.% filler concentrations when subjected to a deformation rate of 200 mm/min. In these instances, the initial upper yield values of 25.6 ± 0.4 MPa were increased to 26.3 ± 0.7 MPa and 28.1 ± 2.8 MPa, correspondingly.

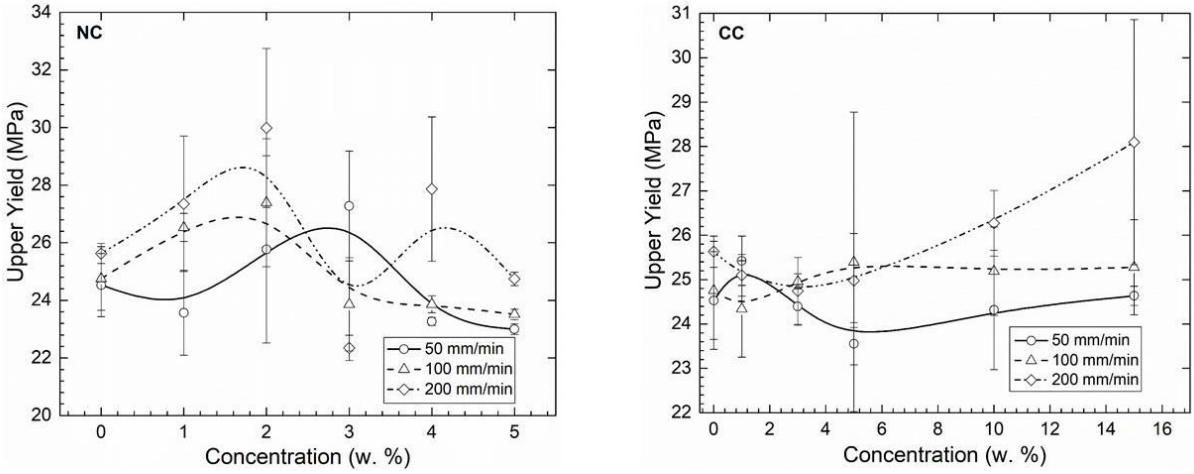

Figure 16. *The CC/HDPE and NC/HDPE composites were found to be dependent on the concentration of inorganic filler and upper yield when subjected to mechanical tensile tests at different strain rates.*

Figure 17 presents the information regarding the relationship between the concentration of fillers and the elongation at break, which has been calculated at various deformation speeds.

The results obtained from the composites made of CC/HDPE showed that as the concentration of filler increased, there was a decrease in the strain at the point of fracture. This implies a decrease in ductility and increased brittle fracture in terms of mechanics models. This supports the well-known principle that polymers with higher crystallinity typically exhibit greater elasticity and stiffness when compared with amorphous methods, which show more plastic behavior. However, in the case of NC/HDPE composites, there was an opposite trend where increasing filler concentration resulted in increased strain before breaking. The reason for this can be explained by how the platelet-shaped nano clay filler particles align themselves at the interface of the polymer chains during the injection molding process.

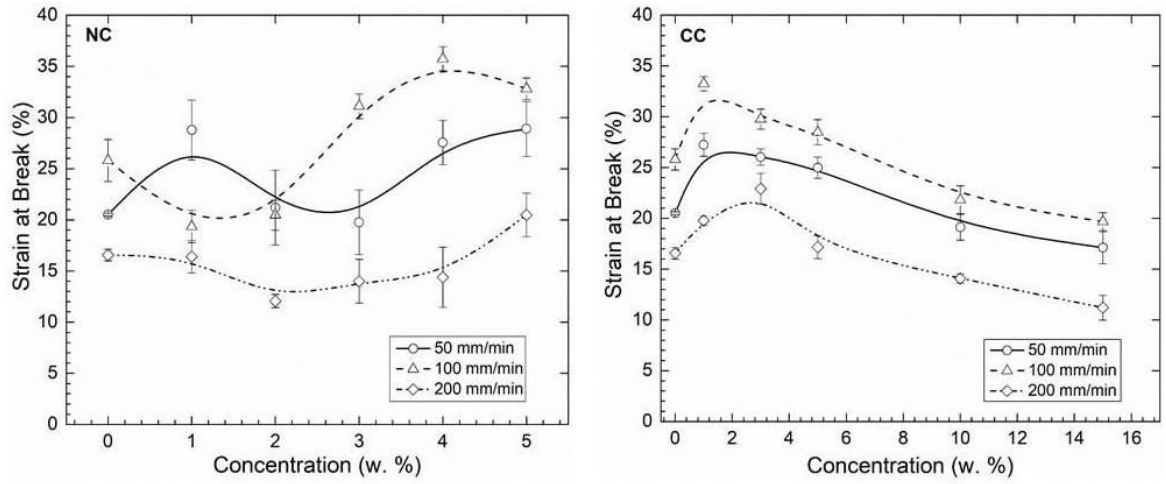

Figure 17. *The mechanical tensile examination of CC/HDPE and NC/HDPE composites at different strain rates determines the elongation at break and nanofiller concentration.*

The analysis of the elongation at break characteristic for 5 wt.% concentrations of nanocomposite fillers, such as nano-clay and nano-calcium carbonate, showed that the composite matrix containing flat-shaped nano clay particles exhibited greater flexibility as compared to the other filler particles at various rates of distortion. The above-mentioned statement is supported by the comparison of the measured values of Young's modulus of elasticity, which demonstrates the CC/HDPE samples had a higher modulus of elasticity than the NC/HDPE samples. Figure 30 illustrates the correlation between the fracture toughness and the concentration of fillers in the composites that were tested. In comparison to the original polymer or virgin one (HDPE), all composite materials exhibited a reduction in fracture toughness. The composite containing 3 wt.% of nano $CaCO_3$ filler had probably the most significant decrease, with a reduction of almost 52.96%. The fracture toughness of NC/HDPE composites was found to be significantly lower, measuring at approximately 22.06 ± 1.42 kJ/m^2.This represents a decrease of about 39.87% in comparison with the original HDPE material. These findings suggest that the composites have an even greater tendency to break easily and exhibit a more brittle behavior when compared with the virgin (Figure 18)

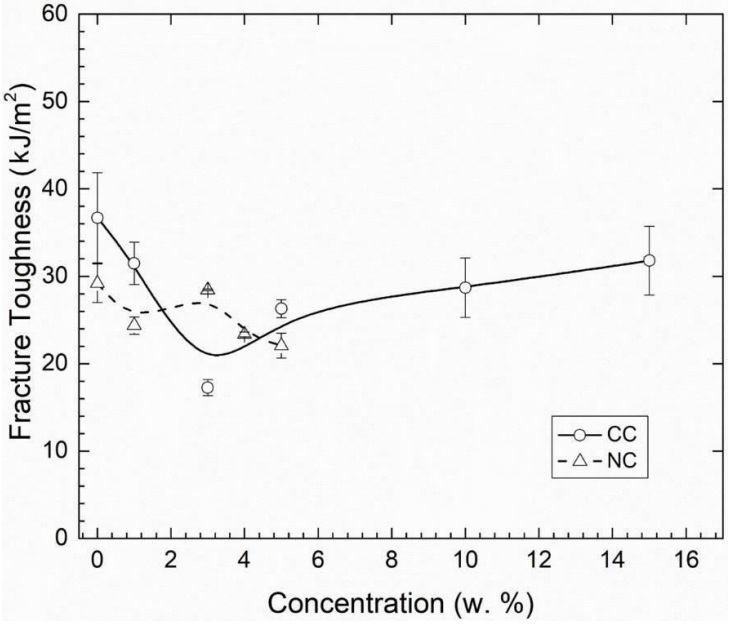

Figure 18. *The Charpy impact test was used to figure out the dependence of fracture toughness and the concentration of fillers in CC/HDPE and NC/HDPE composites.*

The results of the (SFE) calculations are presented in (Table 5), which shows that the addition of $CaCO_3$ and nano clay fillers brought about a decrease in the initial polarity of the pure HDPE material, making it less polar. The measured increase in the dispersive component of surface free energy (SFE) for composite materials containing 5wt.% CC/HDPE increased from 4.19 ± 0.81 mJ/m^2 (pure HDPE) to 39.51 ± 0.63 mJ/m^2. Similarly, for composite materials containing 3 wt.% NC/HDPE, the dispersive component of SFE increased from 4.19 ± 0.81 mJ/m^2 (pure HDPE) to 39.70 ± 1.09 mJ/m^2. The overall surface free energy (SFE) rose significantly in the 5wt % CC/HDPE composites, going from 19.48 ± 2.91 mJ/m^2 (HDPE in its original state) to 32.95 ± 2.58 mJ/m^2, a rise of approximately 103.8%. In the 3 wt.% NC/HDPE composite, the SFE increased by approximately 69.18% to 32.95 ± 2.58 mJ/m^2. The composite interface is now suited for specialized applications like coating or adhesive joints due to its improved adhesive properties, as evidenced by the observed results.

Sample	Surface free energy [mJ/m^2]		
	Total	Polar	Dispersive
HDPE	19.48 ± 2.91	15.29 ± 2.10	4.19 ± 0.81
CC_1%	36.51 ± 33.80	15.61 ± 14.82	15.61 ± 14.82
CC_3%	36.49 ± 14.86	11.84 ± 7.77	24.65 ± 7.08
CC_5%	39.70 ± 1.09	0.19 ± 0.46	39.51 ± 0.63
CC_10%	23.45 ± 4.41	0.01 ± 0.07	23.44 ± 4.34
CC_15%	26.19 ± 0.05	0.41 ± 0.01	25.78 ± 0.03
NC_1%	30.44 ± 1.04	0.12 ± 0.04	30.32 ± 1.00
NC_2%	30.28 ± 0.92	1.19 ± 0.15	29.09 ± 0.76
NC_3%	32.95 ± 2.58	00.08 ± 0.16	32.86 ± 2.42
NC_4%	29.22 ± 0.66	0.22 ± 0.13	29.00 ± 0.53
NC_5%	23.45 ± 4.41	0.01 ± 0.07	23.44 ± 4.34

Table 5. *The Owens, Wendt, Rabel, and Kaelbe method was used to figure out the total surface free energies, as well as the dispersive and polar components, of the HDPE composites being studied. To obtain these measurements, contact angle measurements were taken using axisymmetric drop shape assessment at a temperature of 23°C.*

The data of the micro-indentation testing on the composite substances are shown in (Figure 19) it illustrates the relationship between the indentation modulus and the amount of the filler, as referred to by the E_{IT} pattern. The results display that as the concentrations of the fillers rise, the indentation also increases, confirming that the fillers boost the mechanical properties of the specimens.

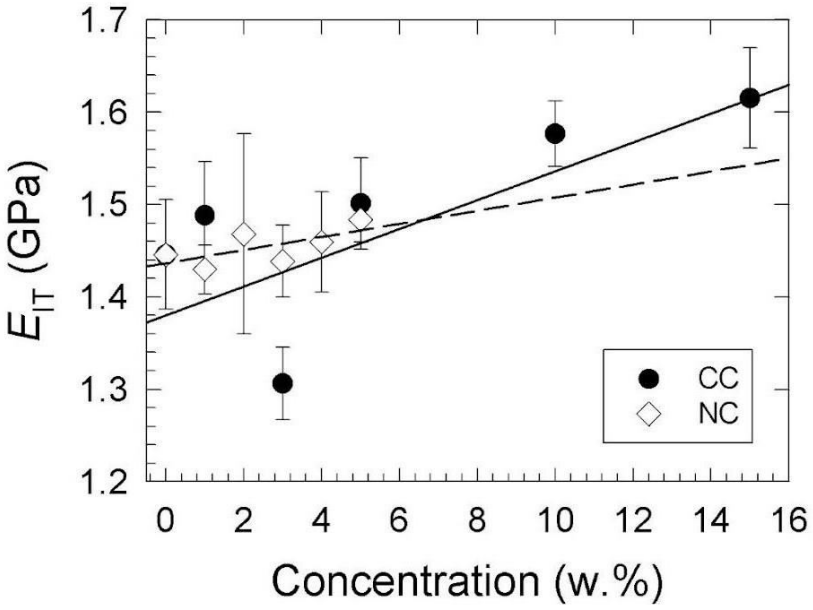

Figure 19. *The relationship between the concentration of fillers and the modulus of indentation (E_{IT}). Type of filler: The Nano $CaCO_3$ has formed a full circle, while the Nano clay remains empty like a diamond. However, a *Point has been deducted due to the lack of linear regression.*

10.2.4 Conclusion

The research examined the physical and mechanical characteristics of HDPE composites that were produced using two distinct types of nano-sized mineral fillers, which is nano clay as well as nano $CaCO_3$. The findings demonstrated that the fillers significantly enhanced the mechanical properties of the composites, including an increase in both the elasticity and indentation strength of 170.4 MPa with regard to the modified HDPE. Nano CC/HDPE composites made up of 5% filler concentrations exhibit strength of 54.7 MPa. Both the nature and amount of the filler had an impact on the plastic-elastic aspects. An increase in the stress level that remains constant and a reduction in the amount of ductility before breaking were signs of this. For both kinds of composites, it was determined that the ideal concentration of filler was 5 weight percent. Furthermore, it was observed that both nanocomposites showed enhanced thermal stability when compared to virgin HDPE, suggesting a far more robust bond with the HDPE matrix. These findings indicate that these nanocomposites might be beneficial for incorporating into complex substance designs, as they exhibit a combination of elastic and plastic mechanical properties across various deformation rates, in addition to improved resistance to changes in temperature.

*****

10.3 Study of mechanical properties of epoxy/graphene and epoxy/halloysite nanocomposites

The aim of research paper D is to contrast the mechanical characteristics of two distinct nanocomposites. Epoxy/Halloysite and epoxy/graphene. Fillers of graphene nanoplatelets (GnPs) and halloysite nanotubes (HNTs) are utilized in the study at various concentrations and are distributed in epoxy resin matrices. The addition of rubber-modified epoxy resin, particularly carboxyl-terminated-butadiene-acrylonitrile copolymer, enhances the characteristics of nanocomposites. During the process of mechanical evaluation, it was found that the hypothesis of individual GnPs particles sliding within the complex resin nanocomposite matrix was supported by the results. The addition of GnPs nanocomposites resulted in enhanced ductility and plasticity, as demonstrated by a 39% increase in elongation at break, which rose from 0.33 mm in the pure matrix to 0.46 mm. Nevertheless, the utilization of HNTs results in a decline in mechanical rigidity, showing a 20% reduction of Young's modulus of elasticity, declining from 3.4 to 2.7 GPa. The research findings suggest that the behavior of the nanocomposites is intricate, involving both brittle and ductile characteristics. This is supported by the measurements of dynamic stiffness. The research indicates that the mechanical characteristics of epoxy-based nanocomposites can be improved by using fillers in a broad sense.

10.3.1 Materials

The investigation utilized a resin known as DGEBA, which is also called laminating resin MGS L285, along with a hardener known as 3-aminomethyl-3,5,5-trimethyl cyclohexylamine. Hexion, (USA) provided two materials, namely L285, as shown in (Figure 20a). The research utilized liquid rubber made from CTBN copolymer, that had been obtained from Zibo Qilong in China. The liquid rubber had an average of 0.58 - 0.65 carboxyl groups per molecule. The molecular weight of the substance was approximately 3,800 Da and it contained 8-12% acrylonitrile, as shown in (Figure 20c). The CTBN technical information is contained in (Table 6). In (Figure 20), the chemical compositions of CTBN, hardener, and epoxy are depicted. The planar shaped GnPs that were used in this study were not functionalized and had an area of 800 square meters per gram, a thickness ranging from 3 to 7 nanometers, as well as an average width of 1.5 meters. The items purchased from (Nano grafi in Ankara, Turkey) were of exceptional quality, and have a purity level of 99.9%. The HNTs that were utilized ($Al_2Si_2O_5(OH)_4$) had a double layer structure that was not cylindrical in form (Esan Eczacibasi, Istanbul, Turkey). The dimensions of the HNTs varied, with an inner diameter ranging from one to 20 nm, an outer diameter ranging from 30 to 50 nm, and a length ranging from 100 to 800 nm.

Parameter	Value
Viscosity (40 °C) (Pa.s)	7 – 12
Carboxyl content (mmol/g)	0.58 – 0.65
Nitrile group content (%)	8.0 – 12.0
Water content (%)	≤ 0.05
Volatile content (%)	≤ 2.0

Table 6. *The liquid rubber CTBN used for application has specific properties.*

10.3.1.1 Preparation of nanocomposites and epoxy blends

10.3.1.1.1 CTBN–epoxy blends

The mixture of epoxy resin and 10 wt.% CTBN liquid rubber was put in a beaker and stirred on a warmed plate to solidify the mixture. Afterward, the resulting mixtures underwent ultrasonication for a duration of 15 to 20 minutes to ensure uniformity. Subsequently, they were degassed in a vacuum oven set at 60°C for a period of 1 hour. The amine-based hardener was added by weight in a proportion of 80:20 (epoxy to hardener) with a slight agitation. After that, the mixtures were poured into molds and left to harden at a temperature of 90°C for one hour. This was followed by an additional 3 hours of post-curing at 120°C. (Figure 20) shows the chemical equations for the epoxy blends used.

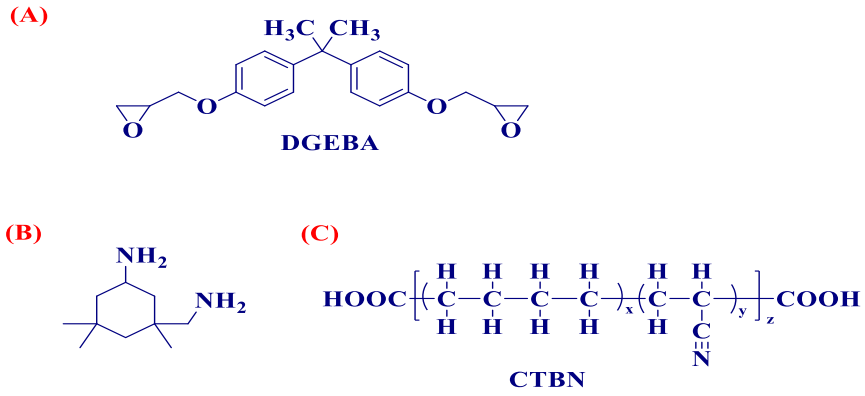

Figure 20. *The build of the substances (a) DGEBA, (b) 3-aminomethyl-3,5,5-trimethylcyclohexylamine, and (c) CTBN as it comes to their chemical composition.*

10.3.1.1.2 CTBN– GnPs–epoxy and CTBN–halloysite–epoxy composites

Previous research determined the nano-reinforcement ratios of epoxy mixtures. A lot of scientists have performed experiments to determine the amount of graphene nanoplatelets (GnPs) and halloysite nanotubes (HNTs) present in the epoxy matrix. The reported concentrations have varied, with GnPs ranging from 0 to 1 weight percent (wt.%) and HNTs

ranging from 0 to 5 (wt.%). The study has checked out how different amounts of fillers affect the tensile, fracture, and flexural properties of the original matrix. In order to create epoxy mixtures containing HNTs and GnPs, SEM images (Figure 21) have been taken of the epoxy resin with varying concentrations of GnPs (0, 0.125, 0.25, 0.5, 0.75, along with 1 wt.%) and HNTs (0, 1, 2, 4, 5, and 5wt.%) as part of the preparation process. The mixtures that were obtained and moved to a RETSCH-PM 100 planetary mill and mixed at a speed of 200 rotations per minute for a duration of 25 hours. The mixing bowls were filled with a combination of epoxy mixtures and balls, resulting in a ratio of 30 balls to every 1 unit of powder. Initially, the mixtures were blended together for a period of 30 minutes. After that, they were allowed to rest for ten minutes in order to prevent excessive heating. Following this, the mixtures were blended once again, and this process was repeated until the desired duration of mixing was achieved. Subsequently, a 10 wt.% of CTBN was incorporated into each epoxy mixture, including those containing GnPs and HNTs. This addition resulted in the formation of composite materials known as CTBN-GnPs-epoxy and CTBN-HNTs-epoxy. After that, the prepared mixtures were stirred using ultrasonication for a duration of 25-30 minutes to achieve uniformity. Afterwards, any gases present were removed by placing the mixtures in a vacuum oven at a temperature of 60°C for approximately 1 hour. In addition, the process of curing CTBN-epoxy blends, as pointed out in (Section 10.3.1.1), was utilized to treat the CTBN-GnPs-epoxy and CTBN-HNTs-epoxy composites. It is important to note that all the epoxy/graphene and epoxy/halloysite nanocomposites that were studied had the same amount of CTBN liquid rubber, which was 10% by weight. However, the original epoxy matrix didn't have exactly the same content (123,124-128).

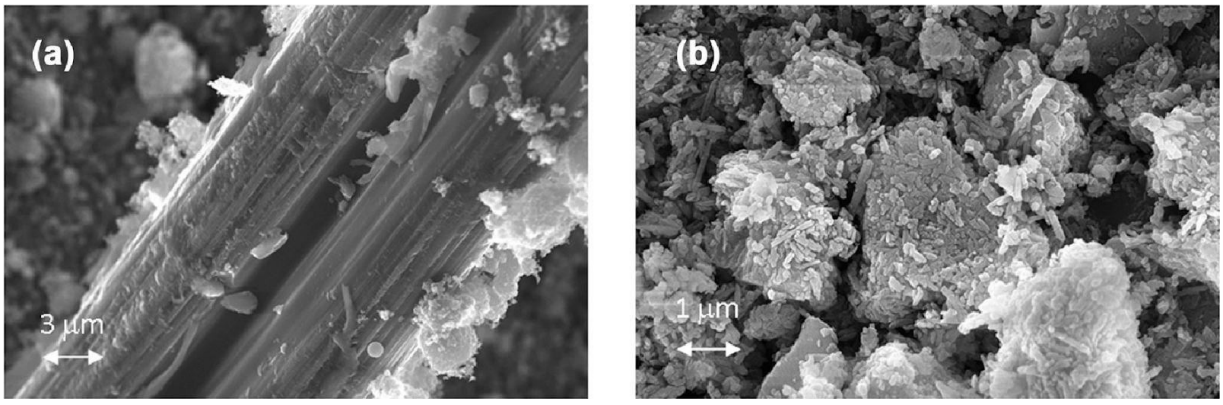

Figure 21. *SEM images displayed the fillers that were analyzed, including GnPs and HNTs.*

10.3.2 Methodology

10.3.2.1 SEM analysis

The examination of SEM was carried out by utilizing a Zeiss EvoLS10 microscope from (Germany) that had an energy dispersive X-ray detector. In order to get the nanofiller samples ready for imaging, the fillers were dispersed in acetone and subjected to ultrasonication for fifteen minutes. The resulting mixture was then poured onto a copper mesh with a regular 400-grid size and left to dry in the air. An accelerating voltage of two kilovolts was utilized to obtain scanning electron microscopy images.

10.3.2.2 Uniaxial tensile testing

The mechanical characteristics of injection-molded samples were evaluated through uniaxial tensile testing, utilizing the universal testing machine Autograph AGS-100 Shimadzu from (Japan) and the Zwick 1456 multipurpose tester from Zwick Roell, Ulm, (Germany). The Compact Thermostatic Chamber TCE Series was incorporated in the Zwick 1456 tester. The tensile test was carried out following the guidelines of' ČSN EN ISO 527-1 and ČSN EN ISO 527-2, with an 80 mm gauge length and a deformation rate of 50 mm/min until the point of fracture. The graphs that depict the relationship between stress and strain were utilized to determine the Young's modulus of elasticity and the point of elongation where the material breaks. A total of ten repetitions were carried out for each study, and afterwards, the average values and standard deviations have been calculated. The experiments were performed at a consistent temperature of 25°C in the laboratory. Nanofiller specimens were placed on a regular copper mesh with a 400-grid pattern to capture SEM images. SEM analysis has been carried out at 2 kilovolts accelerating voltage with a Zeiss EvoLS10 equipped with an energy dispersive X-Ray detector (Germany). The fillers were mixed with acetone and subjected to ultrasonication for 15 minutes. Afterwards, the mixture was poured onto a copper mesh and then allowed to dry in the air. Finally, the samples were examined using scanning electron microscopy (SEM).

10.3.3.3 Charpy impact testing

The Zwick 513 Pendulum Impact Tester from Zwick Roell in Ulm, Germany was used to carry out impact tests following the guidelines of the ČSN EN ISO 179-2 standard, allowing for a 25 J energy release. The fracture toughness was determined by taking the average and standard deviation of 10 repeated experiments. The experiments were all carried out at the typical temperature of the laboratory, which was 25°C.

10.3.3.4 Microhardness

Micro-indentation tests have been performed in accordance with the SN EN ISO 14577 standard using a micro-indentation tester (micro combi tester, Anton Paar, Austria) to determine micro-hardness. The diamond tip utilized had a cube-corner shape and had been created by Vickers, a company based in Austria. The 3 N was determined as the highest weight allowed, with a loading and unloading speed of 6 N per minute, in addition to a duration of 90 seconds for holding. Tests were carried out using the depth sensing indentation technique, which enables the measurement of both the applied force and displacement of the indenter tip at the same time. The calculation of the indentation modulus was derived from the elastic modulus of the strain at a particular level, using a Poisson's ratio within the range of 0.3-0.4 (129,130).

$$E_{IT} = E^{\star}(1 - v^2). \tag{9}$$

In order to guarantee accuracy, the indentation modulus was measured multiple times (10 repetitions) as well as the mean values and standard deviations of these measurements were computed. The laboratory conducted the experiments at its normal temperature of 25°C.

10.3.3.5 Uniaxial 3-point bending tests

The Zwick 1456 testing equipment supplied by Zwick Roell GmbH & Co, KG in Ulm, (Germany) was used to carry out a unidirectional, 3-point bending test in accordance with the ČSN EN ISO 14125 standard. The outcomes were evaluated using TestXpert software. The distance between the supports was found to be 64 mm, and both supports and also the load

mandrel was found to have a circularity of 5 mm. During the 3-point bending experiment, the speed of deformation was established at 1 millimeter per minute, while the pace of loading was established at 50 millimeters per minute.

4.3.3.6 Displacement transmissibility measurements

The Formula (10) (131) is used to compute displacement transmissibility T_d, which is the measurement of displacement.

$$T_d = \frac{y_2}{y_1} = \frac{a_2}{a_1}, \tag{10}$$

The variables y_1 and y_2 represent the intensity of displacement on the input and output sides of the specimen that was tested. The acceleration amplitude on the input side of the tested sample is denoted by a_1, while on the output side, it is denoted by a_2. Equation (11) (132) offers a solution. The transmissibility of displacement for a system consisting of a mass m, a spring with stiffness k, and a damper with damping coefficient c.

$$T_d = \sqrt{\frac{k^2+(c.\omega)^2}{(k-m.\omega^2)^2+(c.\omega)^2}} = \sqrt{\frac{1+(2.\zeta..r)^2}{(1-r^2)^2+(2.\zeta.r)^2}}. \tag{11}$$

The formula (11) enables the case $dT_d/d_r = 0$ to be met and the frequency ratio r_0 can be determined that corresponds to the greatest amount of displacement transmissibility (133,134):

$$r_0 = \frac{\sqrt{\sqrt{1+8.\zeta^2}-1}}{2.\zeta}. \tag{12}$$

The displacement transmissibility of any framework composed of a spring, mass and damper is governed by the Formula (12). When the physical stiffness of an object decreases or the damping ratio improves, the peak of displacement transmissibility moves towards lower frequency ratios. The Formula (12) calculates the frequency ratio r_0 which produces the maximum displacement transmissibility $T_{(dmax)}$. The vibration-induced tests were carried out using the forced oscillation technique. The experiment involved determining the displacement transmissibility (T_d) within a frequency range of 2 to 3,200 Hz. This was achieved using a BK 4810 vibrator, BK 3560-B-030 signal pulse multi-analyzer, as well as BK 2706 power amplifier. Brüel & Kjaer's BK 4393 accelerometers were used to determine the acceleration amplitudes (a_1 and a_2) at the input and output points of the specimens being measured. The specimens that have been analyzed had three different inertial masses placed on them, which were zero g, 90 g, and 500 g. The transmissibility of displacement was determined for every one of these masses. The dimensions of the tested sample were (60mm × 60mm × 3 mm) where a thickness of 3 mm. Five repetitions of all measurements was conducted at a temperature of 22°C, which was the standard.

10.3.4 Results and discussion

Section 10.3.1 demonstrated the typical forms of the nanofillers utilized in this research, as shown in (Figure 21) through SEM analysis. (Figure 21a) shows the GnPs lamellar configuration, which is identifiable by its layer thickness ranging from 3 to 7 nm and a layer width of about 1.5 to 2.0 µm. In contrast, the condensed and aggregation clusters arrangement of HNTs nanotubes (Figure 21b) is made up of separate nanotubes that measure around 30 to 50 nm in diameter and 100 to 800 nm in length. The findings from the tensile-testing trials conducted on the investigated nanocomposites are showcased in (Figure 22) (135). Based on the findings, the Young's modulus of elasticity (E) decreased during uniaxial testing as a result of the rise in the percentage of GnPs filler. The value of the neat matrix dropped from 3.4 GPa to 2.7 GPa with the inclusion of 1 wt.% epoxy and GnPs nanocomposite. The reduction in size was linked to a nonlinear rise in the elongation at the point of fracture, which suggests that the elongation at break increase and consequence the ductility of epoxy/GnPs nanocomposites increased. This phenomenon could be credited for the impact of the GnPs nanofiller molding on the mechanical characteristics of the composite substance. The behavior that was observed was caused by the nanoplatelet sheets sliding into the complex structure of the epoxy/GnP nanocomposite. The reason behind this movement was determined to be due to the bending or turning of cracks, breakage of layers, and the separation or detachment of GnPs layers, as previously mentioned in sources (136,137).

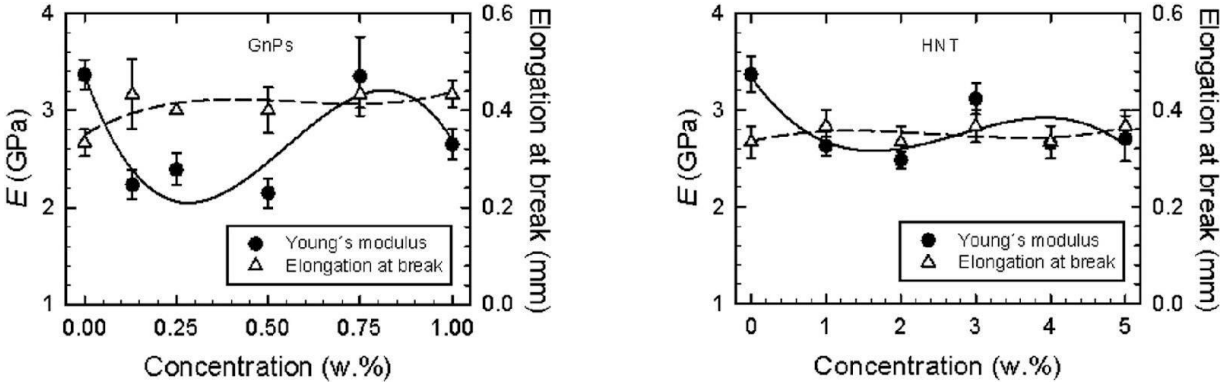

Figure 22. *The connection between Young's modulus of elasticity and also the elongation at break of the investigated nanocomposites containing HNTs and GnPs, taking into account the existence of nanofillers.*

The speed at which the deformation was applied was fifty millimeters every minute. The chart displays a complete line indicating the Young's modulus of elasticity, and a broken line representing the elongation at the point of fracture. In comparison, the mechanical stiffness of the elements studied decreased as seen in the (E) for epoxy/HNT nanocomposites which decreased from 3.4 GPa in the pure matrix to 2.7 GPa in the 5 wt.% epoxy/HNTs nanocomposite. The increase in HNTs filler concentration led to an increased stiffness compared to epoxy/GnPs nanocomposites. The results show that there is a constant relationship between elongation at break, which is around 0.36 mm, and the observed results shown in (Figure 23). The composite material was thought to become a lot more brittle fraction following the addition of HNT nanofiller based on the above data. The HNTs nanofillers were prevented from sliding within the composite matrix, which was linked to this. The results of the uniaxial tensile examinations matched the measurements of fracture toughness (136) in a favorable fashion (Figure 23). At a filler concentration of 1 wt.%, the epoxy/HNTs nanocomposites had a higher fracture toughness of 8.2 kJ/m^2 when compared with the epoxy/GnPs nanocomposites that had a fracture toughness of 6.0 kJ/m^2. The fracture toughness showed a gradual decrease that was not linear when more HNTs filler (1-5 w.%) was added.

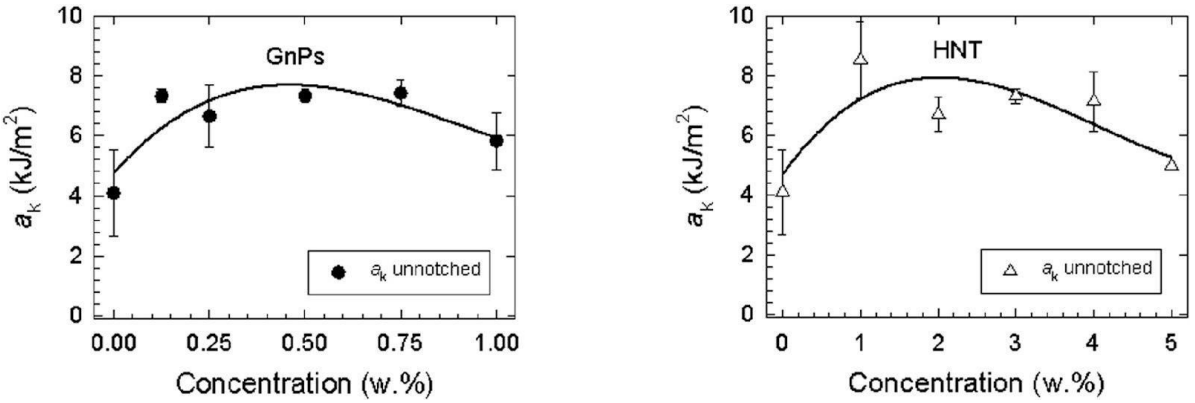

Figure 23. *The dependence of the concentration of the nanofiller on the unnotched fracture hardness of the GnPs and HNTs nanocomposites was investigated.*

The continuous composite matrix was accelerated by CTBN (Figure 21c), which resulted in local deformations in the matrix. The distortion of the matrix mechanisms enabled the spreading of external mechanical energy throughout a significant area, thus hindering the formation of a single brittle crack. To be able to attain the highest level of effectiveness in modifying rubber, specific requirements must be fulfilled, including the establishment of a two-parts structure, sufficient bonding at the interface, and a precise separation distance between adjacent rubber areas (138). According to (139), a similar pattern of conduct was noticed in adaptable polymers that contained both soft and hard components, where the hard parts showed increased stiffness, while the soft parts displayed greater elasticity. (Figure 24) depicts the results obtained from the evaluations of micro-hardness versus filler concentration for the two epoxy nanocomposites that were examined. According to the findings, the indentation modulus EIT experiences a non-linear decrease as the concentration of filler decreases. In relation to the epoxy/GnP nanocomposites, it was noticed that the effective elastic modulus EIT of the material decreased from 4.3 GPa (without any GnPs/pure matrix) to 3.4 GPa (with 1 wt.% GnPs nanocomposite). While studying epoxy/HNTs nanocomposites, researchers noted that the material's EIT decreased from 4.3 GPa (in its pure structure) to 3.8 GPa (when a 5 wt.% HNTs nanocomposite was existing). It was believed that the reduction in surface hardness could be attributed to the plasticizing impact of the nanofillers.

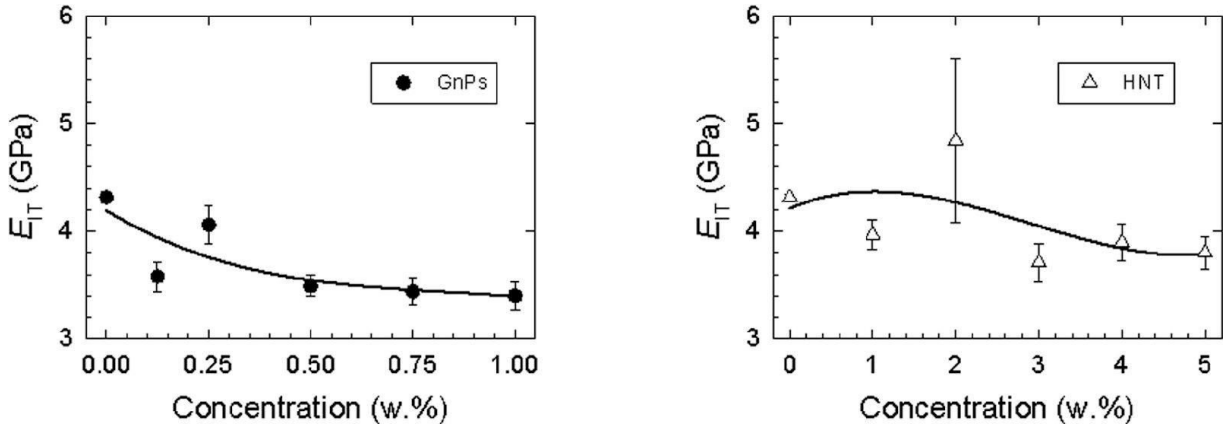

Figure 24. *The relationship between the concentration of nanofillers as well as the indentation modulus of HNTs and GnPs nanocomposites has been examined.*

The results of the 3-point bending tests carried out on the tested nanocomposites are shown in (Figure 25). Brittle materials typically exhibit nonlinear decreasing patterns, which were observed in both nanocomposites under investigation. The research discovered that there was a decrease in the bending modulus (EB) that was not in a straight line as the amount of GnPs filler increased. The bending modulus ranged from 4.3 GPa for the pure matrix to 2.8 GPa for the nanocomposite containing 1 wt.% GnP. The noted occurrence was connected to a consistent and non-linear increase in elongation at the point of fracture, ranging from 5.0 mm (for the pure matrix) to 6.0 mm (for the nanocomposite composed of 1wt.% epoxy and GnPs). The pattern indicates that the composite has increased ductility because of the plasticizing impact of the nanofiller within the prepared epoxy/GnP nanocomposites. On the other hand, the epoxy/HNTs nanocomposites showed a non-linear decrease in EB, going from 4.3 GPa (pure matrix) to 3.0 GPa (in 5wt.% epoxy/HNTs nanocomposites). This indicates that the substances being studied experienced a decrease in their mechanical stiffness. However, there was a small non - linear decrease observed in elongation at break with respect to the amount of HNTs filler present. The break values decreased the elongation from 5.0 mm for pure matrix to 4.1 mm for 5 wt.% epoxy/HNTs nanocomposites. The epoxy/HNTs nanocomposites are found to be more brittle than the epoxy/GnPs nanocomposites, according to the findings.

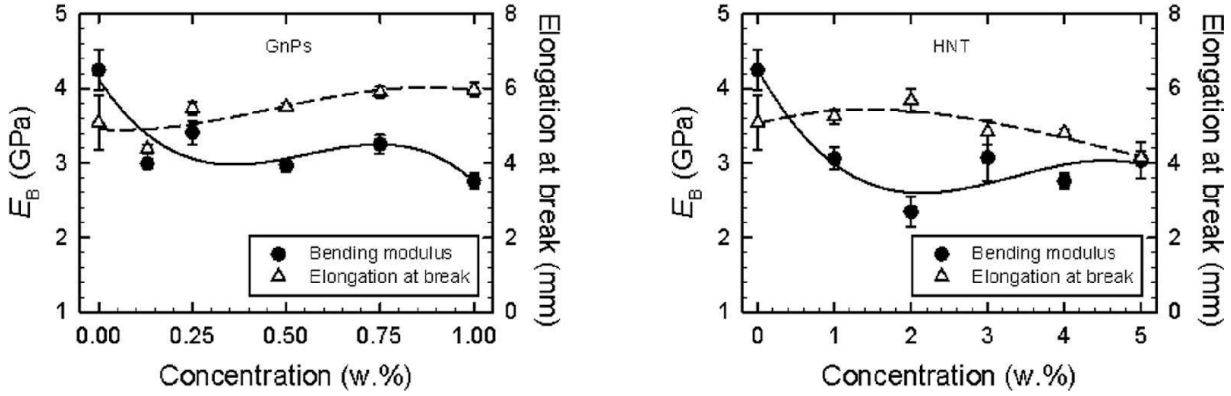

Figure 25. *The concentration of nanofiller was investigated to determine the bending modulus and elongation at the break of HNTs and GnPs nanocomposites. The deformation rate was 50 mm/min. The chart shows two factors, bending modulus, and elongation at break, illustrated by a continuous line and a dotted line, correspondingly.*

The researchers conducted dynamic mechanical evaluations on the nanocomposites being studied, and the results are shown in (Figure 26) and (Figure 27). The frequency connections of displacement transmissibility are depicted in (Figure 26). The results obtained demonstrated a significant degree of similarity with the uniaxial tensile measurements. Figure 26 shows that the displacement of the f_{R1} peak towards higher excitation frequencies is a sign of an increase in material stiffness. A small decrease in the stiffness of the 2nd type was noticed when there were very low amounts of filler present. This was indicated by the minimal shift of f_{R1} towards lower values, as depicted in (Figures 26a) and (Figure 26b). The displacement transmissibility's frequency connections are impacted by the size of the inertial mass, as illustrated in (Figures 26c) and (Figure 38d). According to the research, it was found that an increase in inertial mass resulted in a decrease in the location of the very first resonance frequency peak. As a result, this improved the damping properties of the mechanical vibrations in the components (132).

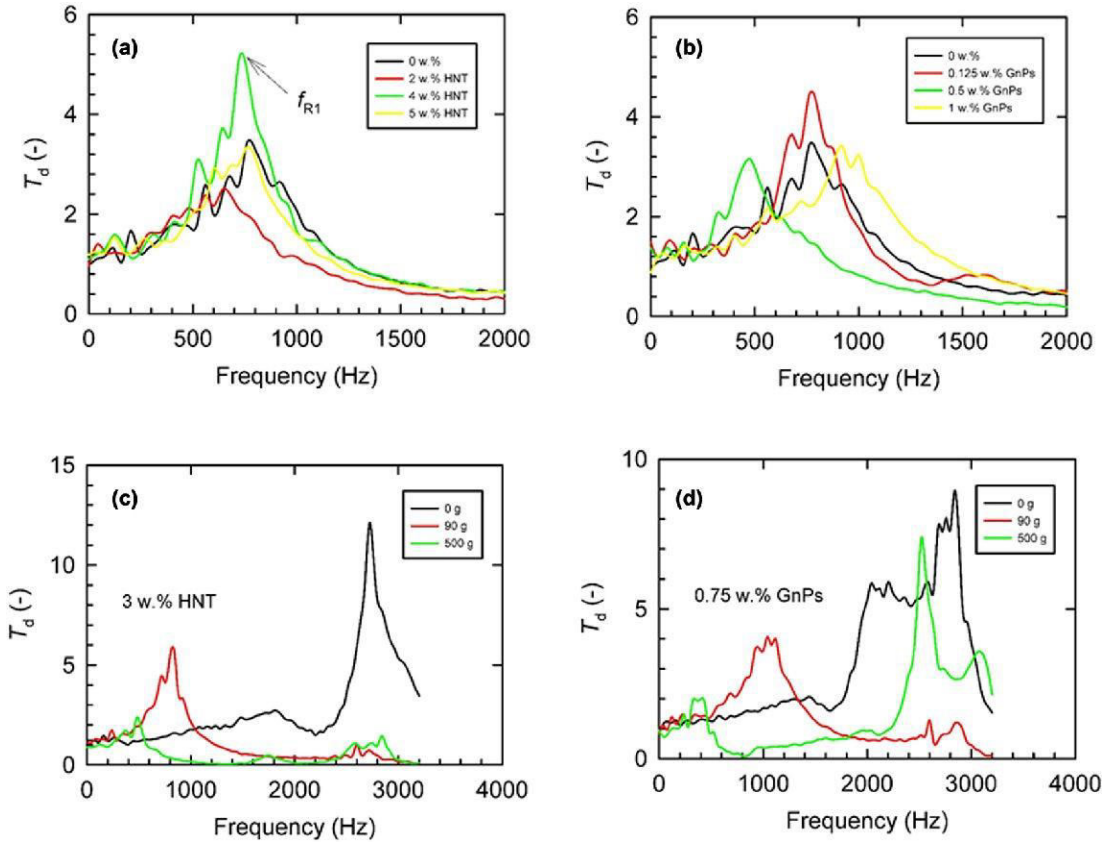

Figure 26. *In order to determine the displacement transmissibility, a comparison was made between the frequency dependencies of the evaluated GnPs and HNTs nanocomposites as shown in the inset a and b. A mass of 90 g inserted in c and d with different concentrations of nanofillers is subjected to inertial forces. The mass that is used in practical applications is related to inertia.*

Furthermore, the rise in f_{R1} with the GnPs concentration validated the enhanced stiffness of the substances, which is consistent with the findings from the prior assessments of the material's tensile strength and fracture toughness as shown in (Figures 22 and 23). The above observations align with the results of the epoxy/GnPs nanocomposite experiment shown in (Figure 27). The experiment demonstrated a clear connection between the concentration of the filler as well as the linear increase of f_{R1} (132). The mechanical stiffness of the epoxy/HNTs nanocomposites decreased as shown by a decrease in f_{R1} and an increase in the concentration of fillers used for the inertial masses, according to (Figure 27) (132).

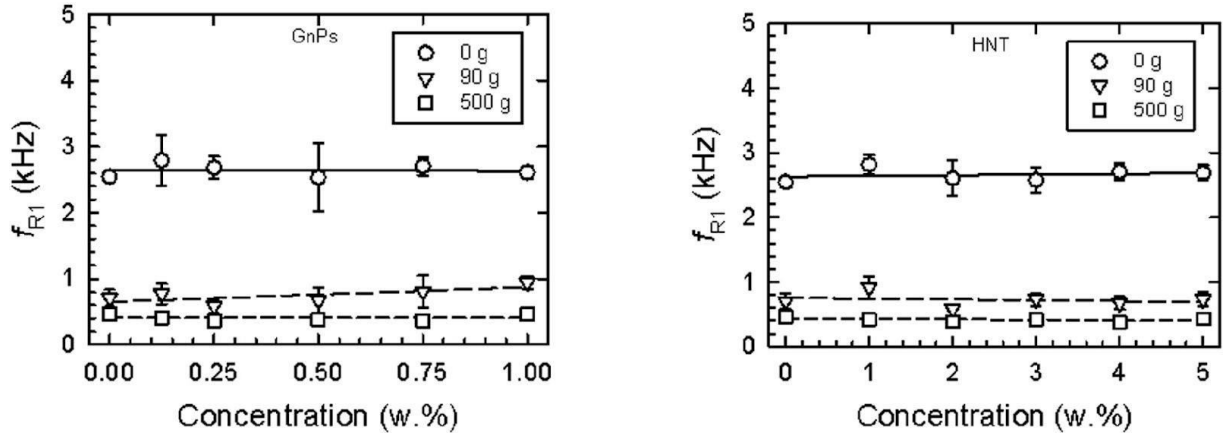

Figure 27. *The concentration dependences of HNTs and GnPs nanocomposites have been compared to their original resonance frequencies. Legend is placed within the graphic.*

10.3.5 Conclusion

The current study has confirmed that it is possible to control the elastic-plastic mechanical properties of complex epoxy resin nanocomposites by using nano-sized GnPs and HNTs fillers. The graph shown in (Figure 22) demonstrates a complex and nonlinear relationship between the concentration of GnPs filler and Young's modulus of elasticity. At exactly the same time, there was an increase in the ductility of the nanocomposites being studied when the concentration of GnPs nanofiller was between 0-1 weight percent. This was demonstrated by the higher elongation at the point of fracture in the specimens, as shown in (Figure 22a). The noted occurrence was ascribed to the interparticle sliding impact demonstrated by the distinct GnPs nanoparticles that dispersed throughout the complex epoxy resin structure. The examination of epoxy/HNTs nanocomposites at concentrations ranging from 1 to 5 wt.% exhibited a steady pattern in Young's modulus of elasticity, with an average value of 2.8 GPa. In addition, (Figure 22) shows that there was a non-linear elongation pattern of approximately 0.35 mm at the point of break. The limited movement of HNTs nanofillers in the matrix is believed to be the root cause of the phenomenon observed during mechanical evaluations. The results of fracture mechanical examinations indicate the rigid epoxy/HNTs nanocomposites tend to be more fracture tough at lower filler concentrations than epoxy/GnPs nanocomposites. This effect can be credited to the GnPs filler's ability to glide and dissipate. The ability of the intricate epoxy/GnPs nanocomposites to change shape and adapt increased as the amount of GnPs filler increased. This was observed through measurements of elongation at break during uniaxial 3-point bending tests. The nanocomposites made of epoxy and HNTs, with a nanofiller concentration of 1 wt.%, exhibited a higher elongation at the point of fracture, measuring 6 mm instead of 5.3 mm. Micro-hardness procedures produced a similar result, with an indentation modulus of 3.4 GPa for epoxy/GnPs nanocomposites compared to 4.0 GPa for epoxy/HNTs nanocomposites (nanofiller concentration 1 wt.%). The epoxy/GnPs nanocomposites appear to have better dissipative mechanical properties, according to this evidence. The previous occurrence was favored to the previously mentioned gliding friction caused by the GnPs nanofiller. The research utilized a distinctive approach to reduce mechanical vibrations, without causing destructive and, by use of forced oscillations. This technique was used to compare the mechanical properties in the low-frequency range of 2-3-200 Hz. The focus was on the location of the initial peak of the resonance frequency. The research verified that epoxy/GnPs nanocomposites exhibited plasticization, as evidenced by a decrease in the position of the very first resonance frequency peak f_{R1} to 2.6 kHz, which was lower than that of epoxy/HNTs nanocomposites, whose f_{R1} magnitude was 2.8 kHz. These two results were acquired when the nanofiller concentration was 1% by weight and there was no inertial mass involved.

*****

10.4 Effect of conditioning on PU foam matrix materials properties

The primary goal of the recently released research article E is to explore the impacts of thermal aging on soft polyurethane foams (PU). Methods including thermal analysis, tensile and compressive testing, and powerful mechanical vibration testing were employed to assess the thermal and mechanical properties. The findings suggest that the physical stiffness of PU foams decreases due to degradation processes caused by an increase in relative humidity in the surrounding atmosphere. The above-mentioned occurrence is credited to the plasticizing of the wall material made of polyurethane foam. As a result, there is a decrease in Young's modulus of elasticity, which leads to an increase in the amount of permanent deformation. The research used a novel approach of vibration damping testing, which does not cause destructive, to confirm the decrease in mechanical stiffness. This decline in stiffness indicates a loss of elasticity due to sample conditioning. The decrease in elastic mechanical performance is further supported by the documented decrease in matrix hardness. The PU foam loses significantly in thermal stability as a result of the conditioning impact.

10.4.1 Materials

The study utilized open-cell soft PU foams that were acquired from a local construction hobby market. The foams had a density of more or less 35.4 grams per cubic centimeter with a tolerance of 0.3 grams per cubic centimeter. Samples of polyurethane, also known as PU, were tested in different shapes and sizes to assess their tensile strength (using dog bone shape), evaluate mechanical vibration, permanent deformation, and measure hardness (using cubic shape). The image depicted in (Figure 28) displays the PU foam utilized in the research. PU foam fragments were utilized for the purpose of thermal analysis. The samples were exposed to various levels of heat (45 and 80°C) and moisture (45 and 80%) for different amounts of time, ranging from 0 to 300 hours, in a controlled environment chamber Discovery 105, Angelantoni test technologies, Massa Martana, (Italy).

Figure 28. *The picture below displays the PU foam material that underwent testing.*

10.4.2 Methodology

The uniaxial tensile testing was conducted using the Autograph AGS-X instrument, which is made by Shimadzu in Kyoto, (Japan). The device had been set up making use of the TCE Series compact thermostatic chamber. Tests were conducted in accordance with ČSN EN ISO 527-1 and 527-2 (140) guidelines, using a deformation rate of 100 mm/min. The study consisted of performing each measurement 10 times and calculating the average results. The research employed a thermal analysis instrument known as SDT 650 Discovery with TRIOS software, which was produced by TA instrument in New Castle, DE, (USA). The instrument was used for conducting DSC/TGA TG and DTA tests simultaneously, and Indium was used as a calibration material for the equipment. Before taking each measurement, the specimens

were placed in an aluminum tray. Consistent observations of weight heat flow and temperature variations were made throughout the experiment. The experiment was carried out in a stationary atmosphere with a heat flow of 10°C a minute, spanning a temperature range of 30 to 300°C. Formula (13) (141) is used to assess the capability of a material to damping mechanically and symmetrical induced vibrations in single-degree-of-freedom (SDOF) systems, which is measured by the dynamic displacement transmissibility Td.

$$T_d = \frac{y_2}{y_1} = \frac{a_2}{a_1} = \sqrt{\frac{k^2+(c\cdot\omega)^2}{(k-m\cdot\omega^2)^2+(c\cdot\omega)^2}} \quad (13)$$

where the variables in this equation are known as follows: y_1 represents the displacement amplitude on the start point of the tested sample, y_2 represents the displacement amplitude on the end point, a_1 represents the acceleration amplitude on the start point, a_2 represents the acceleration amplitude on the end point, k represents the stiffness, c represents the damping coefficient, m represents the mass, and w represents the circular frequency (141,142). The PU foams being studied were assessed for their dynamic mechanical vibration - damping abilities using the technique of forced oscillation (143). The degree of permanent deformation has been assessed by adhering to the' ČSN EN ISO 1856 standard. The block being evaluated had dimensions of 50 mm in length, 50 mm in width, and 50 mm in thickness. The displacement transmissibility Td was evaluated by simulating measurements between the frequency range of 2 Hz and 1000 Hz (144). This evaluation was conducted using the BK 4810 vibrator along with the BK 3560-B-030 signal pulse multi-function analyzer and the BK 2706 force amplifier. The samples under study were tested for both acceleration amplitudes a_1 and a_2. The assessment was carried out using BK 4393 accelerometers made by Brüel & Kjaer located in Nærum, (Denmark) (145). The dimensions of the sample being studied were 60 mm in length, 60 mm in width, and 50 mm in thickness. The average displacement-transmissibility was calculated by measuring it three times at a temperature of 25°C, which is considered normal. The indentation method was used to measure the foam hardness using the standard method A of ČSN EN ISO 2439 (645440) for flexible cellular polymeric materials. The samples went through a compression procedure, leading to a 60% decrease in their initial height. After a period of 30 seconds of deformation, the value of force (N) was computed. The samples were measured to be 50 mm in length, 50 mm in width, and 50 mm in thickness. Five measurements were carried out at specific temperatures of 45 as well as 80°C, along with relative humidity levels of 40 and 80%, each measurement was repeated five times in the experiment. The samples went through a 300-hour conditioning procedure where they were subjected to the same temps and relative humidity levels mentioned earlier. After undergoing conditioning, the samples were positioned in the gap of the pressing device and exposed to a pressure that caused their size to decrease by 50 % from the original measurements. This compression process lasted for 30 minutes. After being compressed, the samples were then released and left unrestricted on the flat surface for 30 minutes. The lasting deformation was measured as a ratio to the original size of the sample, and the thickness was reevaluated at a later time.

10.4.3 Result and discussions

The tensile examination of the PU foam components under investigation is shown in (Figure 29). The study revealed that the cellular components improved in mechanical strength and plasticity after 3 hundred hours of conditioning, when subjected to a temperature of 45°C and a relative humidity of 80%, the sample showed an increase in stress at the point of

rupture by 19%, increasing from 155 kPa to 184 kPa. The ductility also rose from 87% under the given conditions of 45°C temperature and 45% humidity to 114% under the given conditions of 80°C temperature and 45% humidity. The conditioning at 80°C exhibited a correlation that remained relatively stable. The durability of the material improved following a 24-hour period of conditioning at a temperature of 45°C and relative humidity of 80%. However, after 48 hours of conditioning, there was a significant drop in mechanical strength. Nevertheless, it was noticed that there was an increase following 3 hundred hours of conditioning. The behavior mentioned previously indicated that significant changes in the structure, which were caused by cross-linking, occurred after 48 hours of exposure to 80% humidity. If the temperature is 80°C and the humidity is relative 45%, then the fracture stress continued to be fairly constant. An increase of around 10% was noticed when the relative humidity was elevated. The information depicted in (Figure 29) displays a noteworthy rise in the ductility of the PU foam material, suggesting that the PU structure has undergone additional plasticization. The improvement in ductility by 19 % from 87% to 114% after subjecting the foam to a 300-hour treatment at 80°C and 45% relative humidity is attributed to changes in the elasticity of the specific cell walls within the foam matrix. The alteration of the foam structure resulted in a modification of the size of each cell, resulting in a rise in the pressure of the air. A change in the shape of individual cellular components is linked to the alteration in magnitude. Cross-linking (146) and partial hydrolysis (147) might have affected the viscoplastic and viscoelastic properties of the polyurethane (PU) matrix. It was proposed that the swelling of various parts of the cell walls in PU is a complex reaction of the material. It was hypothesized that the primary ways in which mechanical energy was transferred and dissipated were through viscous friction and the stiffness of the walls (148).

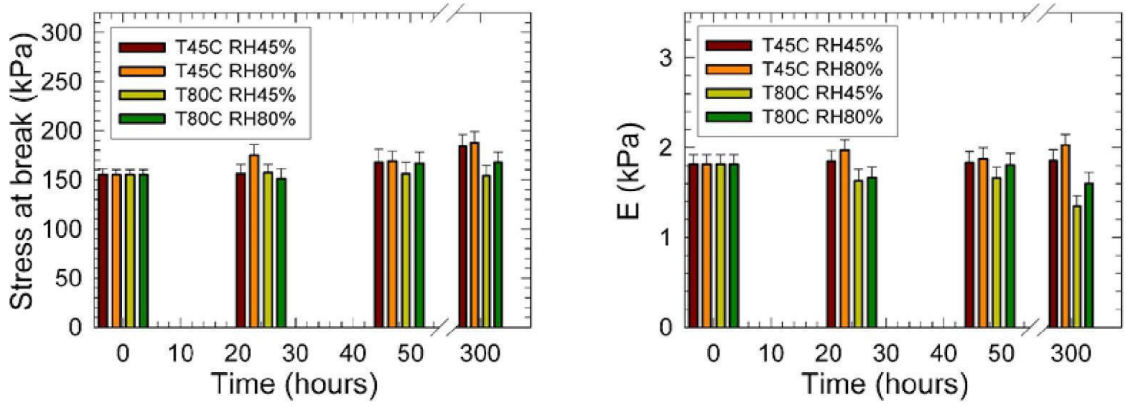

(a) **(b)**

Figure 29. *The results of testing the PU materials being studied through uniaxial tensile evaluation include: (a) determining the stress at which the material breaks and the time it takes to condition at different temperatures and levels of humidity, and (b) determining the elasticity of the material, known as Young's modulus E, while conditioning at different temperatures and levels of humidity. The inset displays the values for T, which represents temperature in degrees Celsius, and RH, which stands for relative humidity in percentage.*

The findings of the research indicate that the increased stress levels observed during the rest of PU samples exposed to 80% relative humidity along with 45°C can be explained by an increase in the stiffness of the structure and the elasticity of Young's modulus. As a result, the brittle pattern of the matrix is enhanced. The research found that signs of matrix hydrolysis were noticed while the conditioning process was carried out at a temperature of 80°C, regardless of the level of relative humidity. The elasticity (E) of the specimen decreased from 1816 Pa (when it was not conditioned) to 1350 Pa (when it had been conditioned at 80°C and

45% relative humidity) and 1600 Pa (when it was conditioned at 80°C and 80% relative humidity). The displacement transmissibility gradually increased with conditioning temperature and relative humidity reaching 80%, according to the results. The PU matrix exhibited greater mechanical stiffness between 250 and 400 Hz, suggesting a higher frequency range. (Figure 30a) illustrates this. A similar result was observed when the conditioning was done at a relative humidity of 40%. According to the hypothesis, the polyurethane matrices that were not reacted completely underwent a chemical process of cross-linking during the first forty-eight hours of conditioning. This supposition is established by the testing methods used in the past to determine tensile strength. The increased relative humidity as shown in (Figure 30b) resulted in the enhancement of Td, which made the improvement in mechanical stiffness of the PU matrix even more noticeable. The findings from (Figure 31a) suggest that there is a significant link between the length of time the foams were conditioned and their level of elasticity. The appearance of 2 peaks in the Td frequencies (occurring at 280 and 430 Hz, with magnitudes of 0.014 and 0.017, respectively) can serve as evidence of this. An increase in stiffness was noticed within the 200 to 600 Hz frequency range, and there have been modifications in mechanical behavior after extended conditioning as shown in (Figure 31b), indicating the presence of plasticity patterns. The foam's elasticity in the frequency range of 200 to 600 Hz was decreased after subjecting it to a 24-hour conditioning period at 80°C and 80% relative humidity, as compared to the initial polyurethane sample. The wall material might have begun to decompose, possibly through hydrolysis.

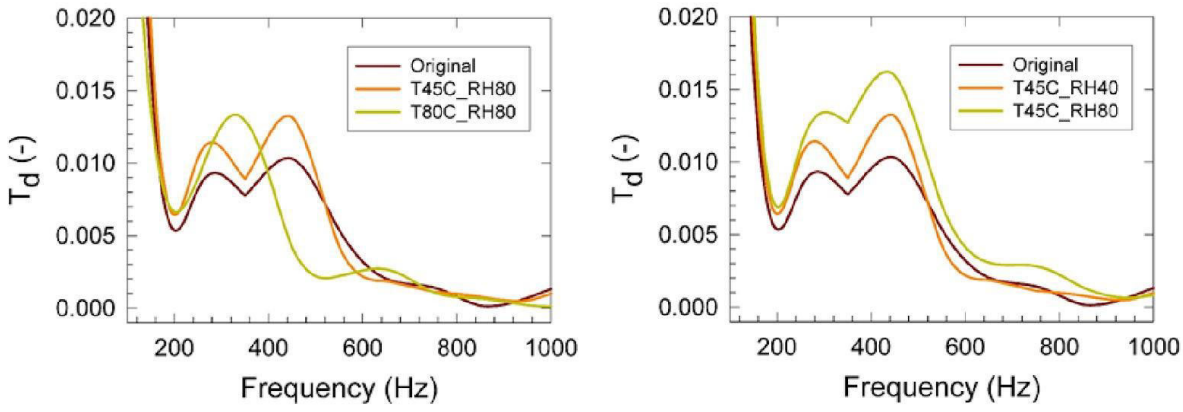

Figure 30. *The relationship between frequency and displacement transmissibility was analyzed using vibration-damping measurements on the PU materials being studied. This was done after a 300-hour conditioning phase, taking into account the impact of both temperature and humidity conditions. Specifically, the effects of conditioning at 80% relative humidity and below 45°C temperature were examined. The original sample without any conditioning is denoted by the variables T for temperature in degrees Celsius and RH for relative humidity in percentage.*

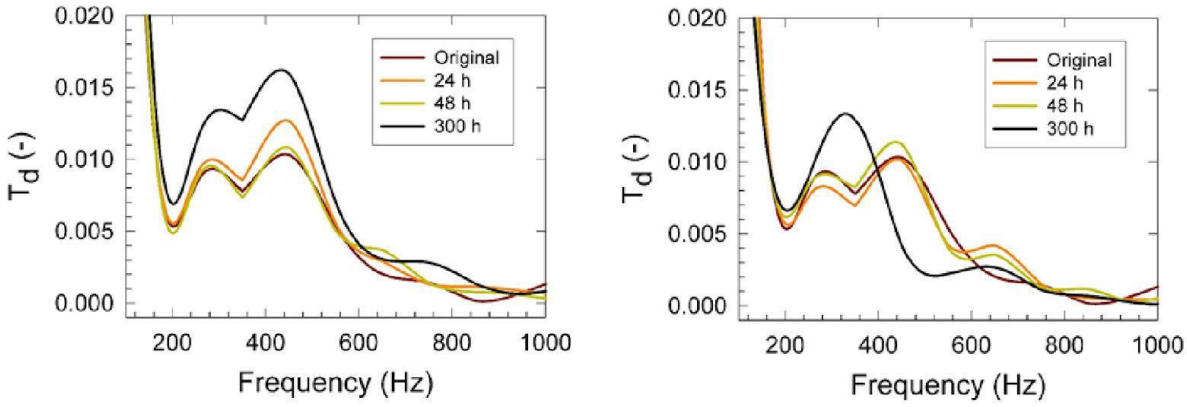

Figure 31. *The examination of the PU substances' oscillation damping demonstrated the correlation between frequency and displacement transmissibility. Figure a display the effects of conditioning time under 45 °C and 80% RH, while Figure b shows the effects of conditioning time under 80°C and 80% RH. The inset indicates the conditioning time in hours, with the original non-conditioned sample.*

The results of sample conditioning on PU foam toughness are shown in (Figure 32). The results indicated that the toughness of all the materials tested decreased, except for those that were subjected to a temperature of 45°C and longer conditioning time. The reduction in hardness observed under the mentioned conditioning details can be attributable to the higher crosslinking density of the PU foam wall matrix. The degree of hardness decreased by 10% to 18% after being conditioned for 300 hours at temperatures between 45°C and 80°C, and with a relative humidity ranging from 45% to 80%. The hardness increased somewhat from 18N to 19 N when relative humidity and the temperature were both 45°C and 45%, respectively. The researchers theorized that the breakdown of PU molecules could be brought on by higher temperatures and increased humidity. Based on Weise et al. (222), crosslinking occurs more frequently in PUs with increased poly(ester) content because ester groups are more prone to hydrolysis than PUs with higher poly(ether) content. The FTIR analysis has confirmed that when ester groups go through hydrolysis, they produce carboxylic acids. These acids then function as unique and non-ductile ionic crosslinks. PU formulations containing only macrodiols experienced a slight rise in mechanical stiffness within the first thousand hours of exposure to weathering. Nevertheless, prolonged contact with weathering led to their eventual deterioration, causing them to weaken to the point of breaking. The results suggest that the deterioration caused a decrease in the mechanical characteristics of poly(ether) type PUs, even though shorter but stiffer crosslinks formed during exposure to weathering.

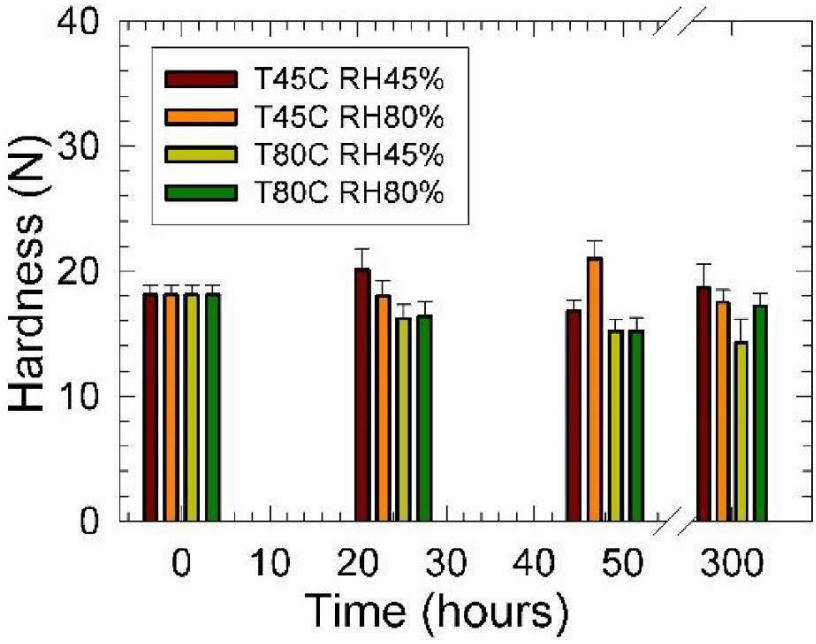

Figure 32. *The correlation between the duration of conditioning and also the level of hardness observed in diverse PU foams under different temperatures and levels of humidity. Inserted: T- represents temperature in degrees Celsius, while RH symbolizes relative humidity in percentage.*

The results shown in (Figure 33) demonstrate that the conditioning temperature plays a significant role in the irreversible deformation of PU foams. In particular, when subjected to a temperature of 45°C during conditioning, there was an increase in elasticity and a decrease in constant deformation when compared with conditioning at higher temperatures. This discovery is in line with the data presented in (Figure 31b), which shows that the Young's modulus of elasticity is greater at lower temperatures of conditioning. The PU foams lasting distortion significantly rose from 18% to 46% as the temperature for conditioning increased from 45°C to 80°C, regardless of the relative humidity. The results showed that the PU foams had a reduced elasticity and an improved plastic mechanical behavior, which were both linked to the reduction in E.

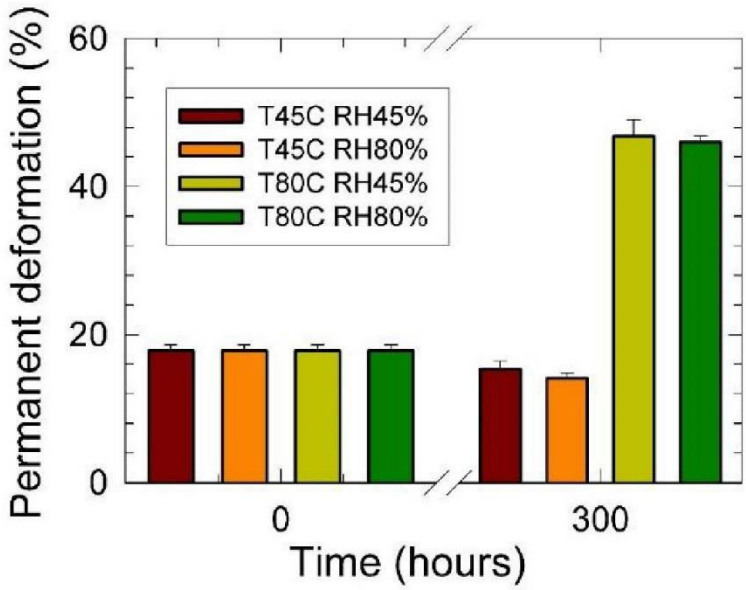

Figure 33. *The relationship between conditioning time and permanent deformation of PU foams is being investigated under different temperature and relative humidity conditions. The inset displays the values for T, which represents temperature in degrees Celsius, and RH, which represents relative humidity in percentage.*

The reference (149) states that single component PUs containing only poly (ester) or poly (ether) macrodiols possess lower mechanical stability than two component PUs containing both macrodiols. The result was a combined effect that resulted in a 24% increase in damping abilities and an 18% enhancement in mechanical strengths after exposure to weather conditions. The enhanced ability of the mixed PUs to absorb vibrations was attributed to a decrease of 15% in the efficiency of the macrodiol chains in packing together, which occurred due to the presence of two different functional groups. The research found that mechanical stabilities increased after weathering, which was due to the combination of the protection and degradation processes of the urethane set by the ester. The degradation structure typically present in the studied polyurethane foams is shown in (Figure 34) and (150,151). The degradation process began at a temperature of 260°C and resulted in a reduction in weight of more or less 86%. Afterwards, there was a release of heat due to the fusion process. The observed deterioration can be explained by the breakdown of the polyurethane material into its individual polyol and also diisocyanate elements. The diisocyanate was then thermally decomposed. The primary substances that were recognized during decomposition were toluene, benzene, phenyl isocyanate, benzonitrile, and methylbenzonitrile. The method of decomposition talked about earlier refers to the process of breaking down diisocyanates and also polyols present in the polyurethane material. This breakdown leads to the emission of carbon dioxide plus hydrogen cyanide gases (152).

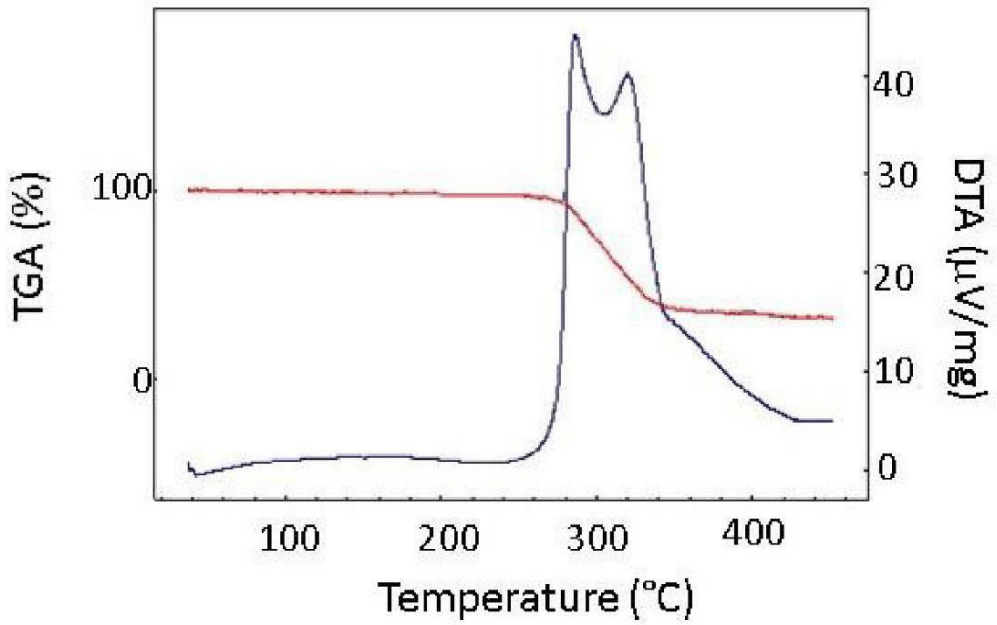

Figure 34. *The red line on the graph signifies the typical thermogravimetric analysis (TGA) pattern observed in the polyurethane foam material. Similarly, the blue line indicates the differential thermal analysis (DTA) pattern observed in the very same material.*

The TGA's evaluation results are briefly summarized in (Figure 35) (152). The empirical evidence suggests that weight loss improves somewhat with increasing conditioning duration, regardless of temperature as well as humidity during conditioning. The alteration in the chemical structure of the polyurethane foam probably resulted in the increase in quantity, perhaps because of the inclusion of unattached isocyanate. The conditioning of PU foam might result in a lessening in its thermal resistance, which is sensible to conclude.

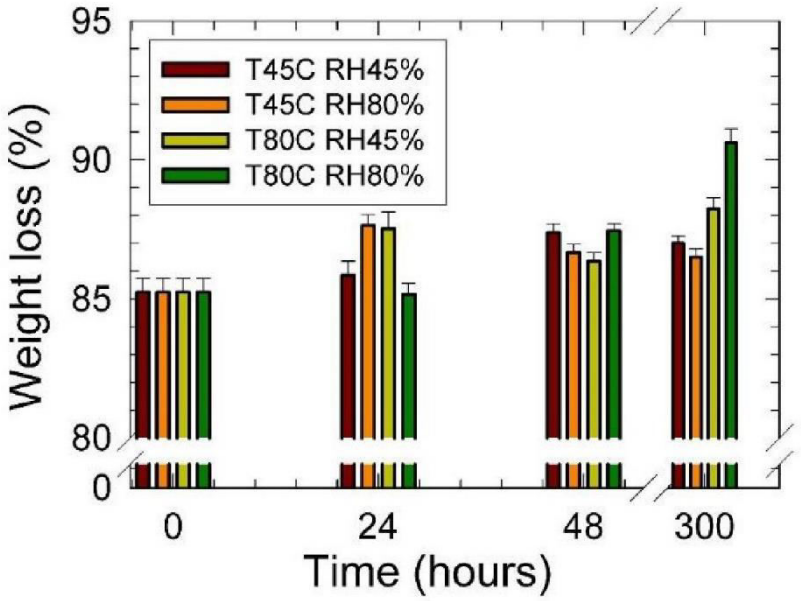

Figure 35. *The PU foams being studied lose weight over time due to conditioning. T-temperature (°C) and RH-relative humidity (%) are shown in the inset.*

10.4.4 Conclusions

The aim of this research was to analyze the physical and chemical characteristics, as well as the mechanical attributes, of commercially available gentle polyurethane foams when subjected to thermal driven degradation. The findings showed that the decline in quality of polyurethane foams began when the temperature and humidity in the surrounding environment increased modulus, the polyurethane foam wall material went through a decrease in stiffnesses due to its plasticization. This was evident from an increment in the constant deformation and dropping in Young's modulus and the elasticity modulus's worth. The phenomenon was even more validated through non - destructive dynamical - mechanical vibration tests, which revealed that the samples exhibited greater vibration damping and reduced elasticity. The decline in the firmness of the matrix was linked to alterations in the mechanical characteristics, suggesting a reduction in the elasticity of the mechanical performance. Moreover, the thermal stability of PU foam was greatly reduced by conditioning.

*****

11. Closing remarks

11.1 Further prospective suggestions for research

The dissertation offers a number of paths for future research and technical progression in the area of polymer nanocomposites. Prospective aspects include the following possibilities:

1) Optimization of filler concentration: Further investigation can focus on enhancing the concentration of fillers in polymer composites to attain the aimed thermal and mechanical features. researchers will be able to gather more comprehensive data and obtain a deeper understanding of the effects of fillers. For specific purposes, it is possible to determine the ideal combination of stiffness, fracture toughness, ductility, along with thermal stability.

2) Investigation of novel fillers: The scope for polymer composites can be expanded by investigating new fillers that possess distinctive characteristics. Scientists have the ability to explore how various forms of nanoparticles, fibers, or several other substances added as fillers can enhance specific characteristics or achieve multiple functionalities. Understanding the way in which polymers interact with matrices and how it affects their thermal and mechanical performance is of utmost importance.

3) Advanced techniques for characterization: can offer more comprehensive understanding of the performance of polymer composites. Advanced microscopy techniques like atomic force microscopy (AFM) and electron microscopy can uncover the microscopic structure and distribution of fillers in the polymer matrix at the nanoscale level. Furthermore, the use of in situ mechanical testing in conjunction with imaging techniques that operate in real-time can enhance comprehension of deformation and failure mechanisms.

4) Fillers that are Sustainable and bio-based: The quest for sustainable and bio-derived substances to use as fillers in polymer composites is gaining greater significance as sustainability becomes a more prominent concern. Investigations can center on the use of fillers obtained from sustainable resources or discarded materials, which can help in the advancement of environmentally friendly and financially feasible composites.

5) Modeling and simulation: Polymer composites and their thermal and mechanical features can be contributed by using modeling and simulation software. By combining empirical data and computer models, the researchers are able to enhance their understanding of the fundamental of the behavior of composite materials in different strategies.

6) Application-based research: Prospective research can be driven by specific needs, such as automotive, aerospace, construction, or biomedical sectors. By tailoring the mechanical and thermal aspects of polymer composites to meet the requirements of these applications, researchers can participate in the development of high-performance, and sustainable substances.

11.2 Final conclusion

The objectives of the dissertation are to improve overall understanding and advancements in technology through the following targets:

1) Exploration of the impact of fillers: The main focus of the thesis is to explore how different fillers, including perlite, nano $CaCO_3$, nano clay, GnPs, and HNTs, impact the

thermal and mechanical characteristics of polymer composites, thereby adding to the general comprehension of this topic. The thesis improves our realization of how fillers and polymer matrices interact by looking at the impacts of these fillers.

2) Mechanical property improvement: The technology is advanced through the examination of how mechanical properties in polymer composites can be improved, as explored in the thesis. The study examines the effects of fillers on Young's modulus of suppleness, elongation at break, fracture toughness and plastic elastic behavior. The examination of the mechanical characteristics of composites can assist in developing materials that possess greater strength and longevity, suitable for a range of uses.

3) Nondestructive testing methods: The technology is enhanced by the thesis through the utilization of non-destructive testing methods such as non-destructive vibrator testing along with dynamic mechanical vibration testing. These techniques provide an understanding of the mechanical behavior of polymer composites without causing any damage. The results will aid in evaluating the reliability and excellence of composite materials in practical situations.

4) The fourth aspect is related to the resistance of a substance to heat and its potential breakdown: The research conducted in the thesis adds to the overall understanding of polymer foams and composites by examining their thermal stability and patterns of degradation. This study investigates how variations in temperature and humidity during conditioning affect the mechanical characteristics and thermal endurance of polyurethane foams. To create products that are more durable and dependable, it is necessary to have an understanding of the ways in which these materials degrade and behave under different temperatures.

In outline: The dissertation's essential argument sets the stage for future investigations into enhancing the amount of filler used, synthesis of novel types of fillers, improving methods for analysis, and creating patterns that account for multiple measurements. These possible topics have the potential to lead progress in the creation and improvement of polymer composites, resulting in boosting features and expanded uses.

*****

List of publications

A. **Murtaja, Y**., Lapčík, L., Lapčíková, B., Gautam, S., Vašina, M., Spanhel, L., & Vlček, J. (2022). Intelligent high-tech coating of natural biopolymer layers. *Advances in colloid and interface science*, *304*, 102681. https://doi.org/10.1016/j.cis.2022.102681. Impact Factor (IF): 15.6

B. Lapčík, L., Vašina, M., Lapčíková, B., Staněk, M., Ovsík, M. & **Murtaja, Y**. (2020). Study of the material engineering properties of high-density poly(ethylene)/perlite nanocomposite materials. *Nanotechnology Reviews*, *9*(1), 1491-1499. https://doi.org/10.1515/ntrev-2020-0113. Impact Factor (IF): 7.848

C. **Murtaja, Y**., Lapčík, L., Sepetcioglu, H., Vlček, J., Lapčíková, B., Ovsík, M. & Staněk, M. (2022). Enhancement of the mechanical properties of HDPE mineral nanocomposites by filler particles modulation of the matrix plastic/elastic behavior. *Nanotechnology Reviews*, *11*(1), 312-320. https://doi.org/10.1515/ntrev-2022-0023. Impact Factor (IF): 7.14

D. Lapčík, L., Sepetcioğlu, H., **Murtaja, Y**., Lapčíková, B., Vašina, M., Ovsík, M., Staněk, M. & Gautam, S. (2023). Study of mechanical properties of epoxy/graphene and epoxy/halloysite nanocomposites. *Nanotechnology Reviews*, *12*(1), 20220520. https://doi.org/10.1515/ntrev-2022-0520. Impact Factor (IF): 7.14

E. Lapčík, L., Vašina, M., Lapčíková, B., & **Murtaja, Y**., (2021). Effect of Conditioning on PU Foam Matrix Materials Properties. *Materials (Basel, Switzerland)*, *15*(1), 195. https://doi.org/10.3390/ma15010195. Impact Factor (IF): 3.748

Conference presentations

I. **Lapčíková, B.**, Lapčík, L., Murtaja, Y., ″Materials characterization of advanced fillers for composites engineering applications″, Poster 58, e-book of Abstracts of 7th International Conference of Engineering Against Failure, June 21-23, 2023, Spetces Island, Greece. Page 72. Conference co-chairmen: Prof. Spiros Pantelakis (University of Patras, Greece) and Prof. Michael Vormwald (TU Darmstadt, Germany).

II. **Lapčík, L.**, Murtaja, Y., Lapčíková, B., ″Study of mechanical properties of epoxy/graphene and epoxy/halloysite nanocomposites″, Oral presentation 65, e-book of Abstracts of 7th International Conference of Engineering Against Failure, June 21-23, 2023, Spetces Island, Greece. Page 83. Conference co-chairmen: Prof. Spiros Pantelakis (University of Patras, Greece) and Prof. Michael Vormwald (TU Darmstadt, Germany).

III. **Murtaja, Y.**, Lapčík, L., Lapčíková, B., ″Study of the material engineering properties of high-density poly(ethylene)/perlite nanocomposite materials″, Oral presentation 73, e-book of Abstracts of 7th International Conference of Engineering Against Failure, June 21-23, 2023, Spetces Island, Greece. Page 93. Conference co-chairmen: Prof. Spiros Pantelakis (University of Patras, Greece) and Prof. Michael Vormwald (TU Darmstadt, Germany).

References

1. Lapcik L, Lapcikova B, Zboril R. Paper-Based Composite Planar Material, EP3034693B1. Munich: European Patent Office; 2018.

2. Lapcik L, Peterkova Petra, Gheorghiu Mihnea. Method of increasing polypropylene biocompatibility by formation of a structured surface layer based on native or modified collagen. CZ-Patent CZ294386,2004.

3. Lapcik L, Lapcik L, Kubicek P, et al. Study of penetration kinetics of sodium hydroxide aqueous solution into wood samples. BioResources 2014;9:881-93.

4. Marchessault RH. All things cellulose: a personal account of some historic events. Cellulose 2011;18:1377-9.

5. Zhang X, Hikal Walid M, Zhang Yue, et al. Direct laser initiation and improved thermal stability of nitrocellulose/graphene oxide nanocomposites. Appl.Phys. Lett. 2013;102:141905.

6. Li A, Wang Yadong, Deng Lijuan, et al. Use of nitrocellulose membranes as a scaffold in cell culture. Cytotechnology 2013;65:71-81.

7. Gao X, Xu Li-Ping, Xue Zhongxin, et al. Dual-scaled porous nitrocellulose membranes with underwater superoleophobicity for highly efficient oil/water separation. Adv Mater 2014;26:1771-5.

8. Stilwell RL, Marks MG, Saferstein L, Wiseman DM. Oxidized cellulose: chemistry, processing and medical applications. Drug Target Recov Handb Biodegr Polym 1997;7:291-306.

9. Kumar V, Yang Tianrun. HNO_3/H_3PO_4-$NaNO_2$ mediated oxidation of cellulose preparation and characterization of bioabsorbable oxidized celluloses in high yields and with different levels of oxidation. Carbohydr Polym 2002;48:403-12.

10. Bajerová Martina, Krejčová´ Kateřina, Rabišková Miloslava, et al. Oxycellulose beads with drug exhibiting pH-dependent solubility. AAPS PharmSciTech 2011;12: 1348-57.

11. Kanmani P, Rhim Jong-Whan. Properties and characterization of bionanocomposite films prepared with various biopolymers and ZnO nanoparticles. Carbohydr Polym 2014;106:190-9.

12. Noreen A, Zia Khalid Mahmood, Tabasum Shazia, et al. Hydroxyethylcellulose-g- poly (lactic acid) blended polyurethanes: preparation, characterization and biological studies. Int J Biol Macromol 2020;151:993-1003.

13. Alekseeva OV, Rodionova Anna N, Bagrovskaya Nadezhda A, Agafonov Alexandr V, Noskov Andrew V. Effect of the bentonite filler on structure and properties of composites based on hydroxyethyl cellulose. Arab J Chem 2019;12:398-404.

14. Lapcik L, Lapcik L, De Smedt S, Demeester J, Chabrecek P. Hyaluronan: preparation, structure, properties, and applications. Chem Rev 1998;98:2663-84.

15. Uyanga KA, Okpozo Oghenefego P, Onyekwere Okwuchi S, Daoud Walid A. Citric acid crosslinked natural bi-polymer-based composite hydrogels: effect of polymer ratio and beta-cyclodextrin on hydrogel microstructure. React Funct Polym 2020; 154:104682.

16. Kupska I, Lapcik L, Lapcikova B, Zakova K, Jurikova J. The viscometric behaviour of sodium hyaluronate in aqueous and KCl solutions. Colloids Surf A Physicochem Eng Asp 2014;454:32-7.

17. Toledo PV, Limeira Diego PC, Siqueira Nicolas C, Petri Denise FS. Carboxymethyl cellulose/poly (acrylic acid) interpenetrating polymer network hydrogels as multifunctional adsorbents. Cellulose 2019;26:597-615.

18. Raab M. Materiály a člověk: (Materiály a člověk: netradiční úvod do současné materiálové vědy). 1999.

19. Lapcík L, Lapcíkov´a Barbora, Stasko Andrej, EPR study of the thermal decomposition of transannular peroxide of anthracene. Int J Org Chem 2011;1:37.

20. Maleki A, Kjøniksen Anna-Lena, Nyström Bo. Effect of shear on intramolecular and intermolecular association during cross-linking of hydroxyethylcellulose in dilute aqueous solutions. J Phys Chem B 2005;109:12329-36.

21. Lei M, Chen Z, Lu H, Yu K. Recent progress in shape memory polymer composites: methods, properties, applications and prospects. Nanotechnol Rev. 2019 Jan;8(1):327-51.

22. Chamis CC. Polymer composite mechanics review – 1965 to 2006. J Reinf Plast Compos. 2007;26(10):987-1019.

23. Singh P, Magalhães Solange, Alves Luis, et al. Cellulose-based edible films for probiotic entrapment. Food Hydrocoll 2019; 88:68-74.

24. Singh N, Hui D, Singh R, Ahuja IPS, Feo L, Fraternali F. Recycling of plastic solid waste: a state of art review and future applications. Compos Part B Eng. 2017 Apr 15;115:409-22.

25. Recycling of plastic solid waste: a state of art review and future applications. Compos Part B Eng. 2017 Apr 15;115:409-22.

26. Mora A, Verma P, Kumar S. Electrical conductivity of CNT/ polymer composites: 3D printing, measurements and modeling. Compos Part B Eng. 2020 Feb 15;183:107600.

27. Mikula M, Čeppan M, Blecha J, Lapcík L, Kalíšek V. Kinetic dissolution measurement of polymers by solution viscosity recording. Polym Test 1988;8: 339-51.

28. Wang X, Xu P, Han R, Ren J, Li L, Han N, et al. A review on the mechanical properties for thin film and block structure char- acterised by using nanoscratch test. Nanotechnol Rev. 2019 Jan;8(1):628-44.

29. Kenisarin MM, Kenisarina KM. Form-stable phase change materials for thermal energy storage. Renew Sustain Energy Rev. 2012 May;16(4):1999-2040.

30. Beesetty P, Kale A, Patil B, Doddamani M. Mechanical behavior of additively manufactured nanoclay/HDPE nanocomposites. Compos Struct. 2020 Sep 1;247:112442.

31. Lopez-Gonzalez M, Flores A, Marra F, Ellis G, Gomez-Fatou M, Salavagione J, et al. Graphene and polyethylene: a strong combination towards multifunctional nanocomposites. Polymers. 2020 Sep;12(9):2094.

32. Privalko E, Pedosenko A, Privalko V, Walter R, Friedrich K. Composition-dependent properties of Polyethylene Kaolin composites. I. Degree of crystallinity and melting behavior of polyethylene. J Appl Polym Sci. 1999 Aug 15;73(7):1267-71.

33. Da Silva A, Rocha M, Moraes M, Valente C, Coutinho F. Mechanical and rheological properties of composites based on polyolefin and mineral additives. Polym Test. 2002 Feb;21(1):57-60.

34. Zhang Y, Shi J, Zheng J. A method of fracture toughness JIC measurement based on digital image correlation and acoustic emission technique. Mater Des. 2021;197.

35. Gill YQ, Jin J, Song M. Comparative study of carbon-based nanofillers for improving the properties of HDPE for potential applications in food tray packaging. Polym Polym Compos. 2020 Oct;28(8-9):562-71.

36. Lapčík L, Maňas D, Vašina M, Lapčíková B, Řezníček M, Zádrapa P. High density poly(ethylene)/CaCO3 hollow spheres composites for technical applications. Compos Part B Eng. 2017 Mar 15;113:218-24.

37. Ehrenstein GW, Riedel G, Trawiel P. Thermal analysis of plastics: theory and practice. Munich: Carl Hanser Verlag; 2004.

38. Sun X, Zhang J. Displacement transmissibility characteristics of harmonically base excited damper isolators with mixed viscous damping. Shock Vibrat. 2013;20(5):921-31.

39. Tu Z, Shim V, Lim C. Plastic deformation modes in rigid poly-urethane foam under static loading. Int J Solids Struct. 2001 Dec;38(50-51):9267-79.

40. Mishra A, Gangele A. Smart materials for clean and sustainable technology for smart cities. Mater Today Proc 2020;29:338-42.

41. Lv J, Liu Zhuoyu, Zhang Jie, Huo Jizhen, Yu Yingfeng. Bio-based episulfide composed of cardanol/cardol for anti-corrosion coating applications. Polymer 2017;121:286-96.

42. Bourbonnais R, Marchessault Robert H. Application of polyhydroxyalkanoate granules for sizing of paper. Biomacromolecules 2010;11:989-93.

43. Hu B. Biopolymer-based lightweight materials for packaging applications. Light Mater Biopolymers Biofibers 2014:239-55.

44. Nicolson PC, Baron Richard Carlton, Chabrecek Peter, et al. Extended wear ophthalmic lens. In: Official Gazette of the United States Patent and Trademark Office Patents; 2017.

45. Chabrecek P, Lohmann D. Surface modification of extended wear contact lenses by plasma-induced polymerization of vinyl monomers. Fundam Appl Asp Chemically Modified Surf 1999:223-34.

46. Marchessault RH. All things cellulose: a personal account of some historic events. Cellulose 2011;18:1377-9.

47. Shao ZQ, Wang WJ. Structure and Properties of Cellulose Nitrate. Beijing: National Defense Industry Press; 2011.

48. Zhang Y, Wang Feijun, Gao Kezheng, Liu Yanhua, Shao Ziqiang. Alcogel and aerogel of nitrocellulose formed in nitrocellulose/acetone/ethanol ternary system. Int J Polym Mater Polym Biomater 2016;65:377-83.

49. Tunç S, Duman Osman. Preparation and characterization of biodegradable methyl cellulose/montmorillonite nanocomposite films. Appl Clay Sci 2010;48: 414-24.

50. Mikula M, Čeppan M, Blecha J, Lapcík L, Kalíšek V. Kinetic dissolution measurement of polymers by solution viscosity recording. Polym Test 1988;8: 339-51.

51. Kalisek V, Lapcik L, Mikulaskova B. Evaluation of the fixation of polyester-based textile materials. III. Influence of the fixation conditions on swelling time and degree of fixation. J Polym Mater 1998;15:299-309.

52. Pelikan P, Čeppan Michal, Liška Marek. Applications of numerical methods in molecular spectroscopy. In: Fundamental & Applied Aspects of Chemometrics Book. 1; 2020.

53. LAPČÍK, Lubomír, Michal ČEPPAN a Peter PELIKÁN. Fotochemické procesy. Bratislava: Alfa, 1989. Edícia literatúry pre spotrebný priemysel (Alfa).

54. Gao J H and Xu B Nano Today 2009;4:37

55. Taniguchi N Ann. CIRF 1983;2:573.

56. Meclean S, Processer E, O'Malley D, Clark N, Ramtoola Z and Brayden D Eur. J. Pharm. Sci. 1998;6:153.

57. Oppenheim R C Int. J. Pharm. 1981;8:217.

58. Kreuter J Pharm. Acta Helv. 1983;58:217.

59. Schafer V, von Briesen H, Andreesen R, Steffan A M, Royer C, Troster S, Kreuter J and Rubsamen-Waigmann H Pharm. Res. 1992;9:541.

60. Narayani R and Rao K P Int. J. Pharm. 1993;95:85.

61. Berthold A, Cremer K and Kreuter J J. Control. Release 1996;39:17.

62. Kreuter J Nanoparticles in Colloidal Drug Delivery Systems (New York: Marcel Dekker) 1994 p 219.

63. Kreuter J J. Drug Target 1995;3:171.

64. Scheffel U, Rhodes B A, Natarajan T K and Wagner H N J. Nucl. Med. 1972;13:498.

65. Birrenbach G and Speiser P J. Pharm. Sci. 1976;65:1763.

66. Kreuter J and Speiser P P Infect. Immun. 1976;13:204.

67. Couvreur P, Kante B, Roland M, Guiot P, Bauduin P and Speiser P J. Pharm. Pharmacol. 1979;31:311.

68. Gurny R Drug Dev. Ind. Pharm. 1981;7:1.

69. Vauthier-Holtzscherer C, Benabbou S, Spenlehauer G, Veillard M and Couvreur P STP Pharm. Sci. 1991;1:109.

70. Allemann E, Leroux J C, Gurny R and Doelker E Pharm. Res. 1993;10:1732.

71. Mathiowitz E et al Nature 1997;386:410.

72. Couvreur P and Vauthier C J. Control. Release 1991;17:187.

73. Couvreur P and Vauthier C Drug Absorption Enhancement Concepts, Limitations and Trends ed A G de Boer (Leiden Amsterdam: Harwood Academic) 1994 p 457.

74. Couvreur P, Dubernet C and Puisieux F Eur. J. Pharm. Biopharm. 1995;41:2.

75. Fattal E, Vauthier C, Aynie I, Nakada Y, Lambert G, Malvy C and Couvreur P J. Control. Release 1998;53:137.

76. Labhasetwar V, Song C and Levy R J Adv. Drug Deliv. Rev. 1997;24:63.

77. Maassen S, Fattal E, Müller R H and Couvreur P STP Pharma. 1993;3:11.

78. Fernandez-Urrusuno R, Fattal E, Porquet D, Feger J and Couvreur P Toxicol. Appl. Pharmacol. 1995;130:272.

79. Emile C, Bazile D, Herman F, Helene C and Veillard M Drug Deliv. 1996;3:187.

80. Rajaonarivony M, Vauthier C, Couarraze G, Puisieux F and Couvreur P J. Pharm. Sci. 1993;82:912.

81. Wang N and Wu X S Pharm. Dev. Technol. 1997;2:135.

82. Calvo P, Remunan-Lopez C, Vila-Jato J L and Alonso M J Pharm. Res. 1997;14:1431.

83. Kumaresh S S, Tejraj M A, Anandrao R K and Walter E R J. Control. Release 2001;70:1.

84. Mua L and Seowc P H Colloids Surf. B 2006;47:90.

85. Couvreur P, Gref R, Andrieux K and Malvy C Prog. Solid State Chem. 2006;34:231.

86. Harito C, Bavykin DV, Yuliarto B, Dipojono HK, Walsh FC Polymer nanocomposites having a high filler content: synthesis, structures, properties, and applications. Nanoscale 2019;11:4653-4682.

87. Hashim AA Polymer thin films. Published by In-Teh In-Teh Olajnica 19/2, 32000 Vukovar, Croatia 2010.

88. Alonso-Redondo E, Belliard L, Rolle K, Graczykowski B, Tremel W, Djafari-Rouhani B, Fytas G Robustness of elastic properties in polymer nanocomposite films examined over the full volume fraction range. Sci Rep 2018; 8:16986.

89. Blattmann CO, Pratsinis SE Single-step fabrication of polymer nanocomposite films. Materials., 2018;11.

90. Begam N, Nimmi Das A, Chandran S, Ibrahim M, Padmanabhan V, Sprung M, Basu JK Nanoparticle-polymer interfacial layer properties tune fragility and dynamic heterogeneity of a thermal polymer nanocomposite films, royal society of chemistry. Soft Matter 2018; 14:8853-8859.

91. Mishra R, Militky J (2019) Nanocomposites. In: Nanotechnology in textiles theory and application. The textile institute book series. pp 263-310, Elsevier.

92. Nanotechnologies-Terminology and definitions for nano-objects-Nanoparticle, nanofibre and nanoplate, ISO/TS 27687:2008. [Accessed March 30,2015]. Iso.org. 26-1-2012. Ref Type: Electronic Citation.

93. Fabbri, P.; Messori, M., Surface Modification of Polymers: Chemical, Physical, and Biological Routes. In Modification of Polymer Properties, Jasso-Gastinel, C. F.; Kenny, J. M., Eds. William Andrew Publishing: 2017; 5:109-130.

94. Lapcik L, Vasina M, Lapcikova B, Hui D, Otyepkova E, Greenwood RW, et al. Materials characterization of advanced fillers for composites engineering applications. Nanotechnol Rev. 2019 Jan;8(1):503-12.

95. Lapčík L, Maňas D, Vašina M, Lapčíková B, Řezníček M, Zádrapa P. High density poly(ethylene)/CaCO3 hollow spheres composites for technical applications. Compos Part B Eng. 2017 Mar 15;113:218-24.

96. Ehrenstein GW, Riedel G, Trawiel P. Thermal analysis of plastics: theory and practice. Munich: Carl Hanser Verlag; 2004.

97. Cuadri AA, Martin-Alfonso JE. The effect of thermal and thermo-oxidative degradation conditions on rheological, chemical and thermal properties of HDPE. Polym Degrad Stab. 2017 Jul;141:11-8.

98. Schawe JEK. Elastomers Vol 1. Mettler-Toledo collected appli- cations. Schwerzenbach: Mettler-Toledo; 2002.

99. Lapcik L, Manas D, Lapcikova B, Vasina M, Stanek M, Cepe K, et al. Effect of filler particle shape on plastic-elastic mechan- ical behavior of high-density poly(ethylene)/mica and poly (ethylene)/wollastonite composites. Compos Part B Eng. 2018 May 15;141:92-9.

100. Rao SS. Mechanical vibrations, 5th edn. Upper Saddle River, USA: Prentice Hall; 2010.

101. Carrella A, Brennan MJ, Waters TP, Lopes V. Force and dis- placement transmissibility of a nonlinear isolator with high- static-low-dynamic-stiffness. Int J Mech Sci. 2012 Feb;55(1):22-9.

102. Ab Latif N, Rus AZM. Vibration transmissibility study of high-density solid waste biopolymer foam. J Mech Eng Sci. 2014;6:772-81.

103. Liu K, Liu J. The damped dynamic vibration absorbers: revisited and new result. J Sound Vibrat. 2005 Jun 21;284(3–5):1181-9.

104. Hadas Z, Ondrusek C. Nonlinear spring-less electromagnetic vibration energy harvesting system. Eur Phys J Spec Top. 2015 Nov;224(14–15):2881-96.

105. Sun X, Zhang J. Displacement transmissibility characteristics of harmonically base excited damper isolators with mixed viscous damping. Shock Vibrat. 2013;20(5):921-31.

106. Tang B, Brennan MJ. A comparison of two nonlinear damping mechanisms in a vibration isolator. J Sound Vibrat. 2013 Feb 4;332(3):510-20.

107. Krasny I, Lapcik L, Lapcikova B, Greenwood RW, Safarova K, Rowson NA. The effect of low temperature air plasma treat- ment on physico-chemical properties of kaolinite/polyethy- lene composites. Compos Part B Eng. 2014 Mar;59:293-9.

108. Lapcik L, Cetkovsky V, Lapcikova B, Vasut S. Materials for noise and vibration attenuation. Chem Listy. 2000;94(2):117-22.

109.Vasina M, Hughes DC, Horoshenkov KV, Lapcik L. The acoustical properties of consolidated expanded clay granulate. Appl Acoust. 2006 Aug;67(8):787-96.

110. Tu Z, Shim V, Lim C. Plastic deformation modes in rigid polyurethane foam under static loading. Int J Solids Struct. 2001 Dec;38(50–51):9267-79.

111. Bernardo V, Laguna-Gutierrez E, Lopez-Gil A, Angel Rodriguez-Perez M. Highly anisotropic crosslinked HDPE foams with a controlled anisotropy ratio: production and characterization of the cellular structure and mechanical properties. Mater Des. 2017 Jan 15;114:83–91.

112. Sepet H, Aydemir B, Tarakcioglu N. Evaluation of mechanical and thermal properties and creep behavior of micro-and nano- CaCO(3) particle-filled HDPE nano- and microcomposites produced in large scale. Polym Bull. 2020;77:3677–95.

113. Se pet H, Tarakcioglu N, Misra RDK. Investigation of mechan- ical, thermal and surface properties of nanoclay/HDPE nano- composites produced industrially by melt mixing approach. J Composite Mater. 2016;50:3105-16.

114. Sepetcioglu H. The effect of nanoclay on the nonlinear vis- coelastic behavior of high-density polyethylene. Polym Compos. 2021;42:3481.

115. Sepet H, Tarakcioglu N, Misra RDK. Determination of the mechanical, thermal and physical properties of nano-CaCO3 filled high-density polyethylene nanocomposites produced in an industrial scale. J Composite Mater. 2016;50:3445-56.

116. Kwok D. The usefulness of the Lifshitz-van der Waals/acid- based approach for surface tension components and interfacial tensions. Colloid Surf A-Physicochem Eng Asp. 1999;156:191-200.

117. Gajdosikova R, Lapcikova B, Lapcik L. Surface phenomena and wetting of porous solids. Phys Chem: Indian J. 2011;6:146-62.

118. Oliver W, Pharr G. Measurement of hardness and elastic modulus by instrumented indentation: advances in under- standing and refinements to methodology. J Mater Res. 2004;19:3-20.

119. Manas D, Mizera A, Manas M, Ovsik M, Hylova L, Sehnalek S, et al. Mechanical properties changes of irradiated thermo- plastic elastomer. Polymers. 2018;10:87.

120. Lapcik L, Manas D, Lapcikova B, Vasina M, Stanek M, Cepe K, et al. Effect of filler particle shape on plastic-elastic mechan- ical behavior of high-density poly(ethylene)/mica and poly (ethylene)/wollastonite composites. Compos Pt B-Eng. 2018;141:92-9.

121. Lapčík L, Maňas D, Vašina M, Lapčíková B, Řezníček M, Zádrapa P. High density poly(ethylene)/CaCO3 hollow spheres composites for technical applications. Compos Pt B-Eng. 2017;113:218-24.

122. Bucknall CB. Toughened plastics. Dordrecht: Springer Science + Business Media, B.V.; 1977.

123. Hashmi MA. Enhancement of mechanical properties of epoxy/halloysite nanotube (HNT) nanocomposites. SN Appl Sci. 2019;1(4):1-8.

124. Srivastava S, Pandey A. Mechanical behavior and thermal stability of ultrasonically synthesized halloysite-epoxy composite. Compos Commun. 2019 Feb;11:39-44.

125. Alexopoulos ND, Paragkamian Z, Poulin P, Kourkoulis SK. Fracture related mechanical properties of low and high gra- phene reinforcement of epoxy nanocomposites. Compos Sci Technol. 2017 Sep 29;150:194-204.

126. Wei JC, Atif R, Vo T, Inam F. Graphene nanoplatelets in epoxy system: Dispersion, reaggregation, and mechanical properties of nanocomposites. J Nanomater. 2015;2015:(3):1-12.

127. Chatterjee S, Nafezarefi F, Tai NH, Schlagenhauf L, Nuesch FA, Chu B. Size and synergy effects of nanofiller hybrids including graphene nanoplatelets and carbon nanotubes in mechanical properties of epoxy composites. Carbon. 2012 Dec;50(15):5380-6.

128. Alamri H, Low IM. Microstructural, mechanical, and thermal characteristics of recycled cellulose fiber-halloysite-epoxy hybrid nanocomposites. Polym Compos. 2012 Apr;33(4):589-600.

129. Oliver WC, Pharr GM. Measurement of hardness and elastic modulus by instrumented indentation: Advances in under- standing and refinements to methodology. J Mater Res. 2004 Jan;19(1):3-20.

130. Manas D, Mizera A, Manas M, Ovsik M, Hylova L, Sehnalek S, et al. Mechanical properties changes of irradiated thermo- plastic elastomer. Polymers. 2018 Jan;10(1):87.
203. Rao SS. Mechanical vibrations. 5th edn. Upper Saddle River, USA: Prentice Hall; 2010.

131. Lapcik L, Vasina M, Lapcikova B, Stanek M, Ovsik M, Murtaja Y. Study of the material engineering properties of high-density poly(ethylene)/perlite nanocomposite materials. Nanotechnol Rev. 2020 Jan;9(1):1491-9.

132. Carrella A, Brennan MJ, Waters TP, Lopes V, Jr. Force and displacement transmissibility of a nonlinear isolator with high-static-low-dynamic-stiffness. Int J Mech Sci. 2012;55(1):22-9.

133. Ab Latif N, Rus AZM. Vibration transmissibility study of high-density solid waste biopolymer foam. J Mech Eng Sci. 2014;6:772-81.

134. Murtaja Y, Lapcik L, Sepetcioglu H, Vlcek J, Lapcikova B, Ovsik M, et al. Enhancement of the mechanical properties of HDPE mineral nanocomposites by filler particles modulation of the matrix plastic/elastic behavior. Nanotechnol Rev. 2022 Jan 5;11(1):312-20.

135. Vijayan PP, George JS, Thomas S. The effect of polymeric inclusions and nanofillers on cure kinetics of epoxy resin: A review. Polym Sci Ser A. 2021 Nov;63(6):637-51.

136. Wang FZ, Drzal LT, Qin Y, Huang ZX. Enhancement of fracture toughness, mechanical and thermal properties of rubber/ epoxy composites by incorporation of graphene nanoplatelets. Compos Part A Appl Sci Manuf. 2016 August;87:10-22.

137. Lapcik L, Raab M. Materials Science II. Textbook. 2nd edn. Zlin: Tomas Bata University in Zlin; 2004.

138. Chen FX, Fan JT, Hui DV, Wang C, Yuan FP, Wu XL. Mechanisms of the improved stiffness of flexible polymers under impact loading. Nanotechnol Rev. 2022 Dec 16;11(1):3281-91.

139. Lapcik, L.; Manas, D.; Lapcikova, B.; Vasina, M.; Stanek, M.; Cepe, K.; Vlcek, J.; Waters, K.E.; Greenwood, R.W.; Rowson, N.A. Effect of filler particle shape on plastic-elastic mechanical behavior of high density poly(ethylene)/mica and poly(ethylene)/wollastonite composites. Compos. Part B Eng. 2018, 141, 92-99.

140. Rao, S.S. Mechanical Vibrations, 5th ed.; Prentice Hall: Upper Saddle River, NJ, USA, 2010; p. 1105.

141. Liu, K.; Liu, J. The damped dynamic vibration absorbers: Revisited and new result. J. Sound Vib. 2005, 284, 1181-1189.

142. Hadas, Z.; Ondrusek, C. Nonlinear spring-less electromagnetic vibration energy harvesting system. Eur. Phys. J.-Spec. Top. 2015,224,2881-2896.

143. Carrella, A.; Brennan, M.J.; Waters, T.P.; Lopes, V., Jr. Force and displacement transmissibility of a nonlinear isolator with high-static-low-dynamic-stiffness. Int. J. Mech. Sci. 2012,55,22-29.

144. Dupuis, R.; Duboeuf, O.; Kirtz, B.; Aubry, E. Characterization of Vibrational Mechanical Properties of Polyurethane Foam. Dyn. Behav. Mater. 2016, 1, 123-128.

145. Lapcik, L.; Vasina, M.; Lapcikova, B.; Stanek, M.; Ovsik, M.; Murtaja, Y. Study of the material engineering properties of high-density poly(ethylene)/perlite nanocomposite materials. Nanotechnol. Rev. 2020,9,1491-1499.

146. Platonova, E.; Chechenov, I.; Pavlov, A.; Solodilov, V.; Afanasyev, E.; Shapagin, A.; Polezhaev, A. Thermally Remendable Polyurethane Network Cross-Linked via Reversible Diels-Alder Reaction. Polymers 2021,13,1935.

147. Nemade, A.M.; Mishra, S.; Zope, V.S. Kinetics and Thermodynamics of Neutral Hydrolytic Depolymerization of Polyurethane Foam Waste Using Different Catalysts at Higher Temperature and Autogenious Pressures. Polym. Plast. Technol. Eng. 2010,49,83-89.

148. Casati, F.; Herrington, R.; Broos, R.; Miyazaki, Y. Tailoring the performance of molded flexible polyurethane foams for car seats (Reprinted from Polyurethanes World Congress ′97, 29 September–1 October 1997). J. Cell. Plast. 1998,34,430-466.

149. Weise, N.K.; Bertocchi, M.J.; Wynne, J.H.; Long, I.; Mera, A.E. High performance vibrational damping poly(urethane) coatings: Blending ‘soft’ macrodiols for improved mechanical stability under weathering. Prog. Org. Coat. 2019,136,105240.

150. Gaboriaud, F.; Vantelon, J.P. Thermal-Degradation of Polyurethane Based on Mdi and Propoxylated Trimethylol Propane. J. Polym. Sci. Part A Polym. Chem. 1981,19,139-150.

151. Ballistreri, A.; Foti, S.; Maravigna, P.; Montaudo, G.; Scamporrino, E. Mechanism of Thermal-Degradation of Polyurethanes Investigated by Direct Pyrolysis in the Mass-Spectrometer. J. Polym. Sci. Part A Polym. Chem. 1980, 18, 1923-1931.

152. Tomin, M.; Kmetty, A. Polymer foams as advanced energy absorbing materials for sports applications-A review. J. Appl. Polym. Sci. 2022,139,51714.